“Babes-Bolyai” University, Cluj-Napoca
Faculty of Chemistry and Chemical Engineering

POP Monica Loredana

Quantum modelling and topology of some non-IPR fullerenes

Ph.D. Thesis Abstract

Scientific advisor:
Prof. dr. Mircea V. Diudea

Cluj-Napoca
-2012-

UNIUNEA EUROPEANĂ
GUVERNUL ROMÂNIEI MINISTERUL MUNCII, FAMILIEI ŞI PROTECŢIEI SOCIALE AMPOSDRU
Fondul Social European POSDRU 2007-2013
Instrumente Structurale 2007-2013
MINISTERUL EDUCAŢIEI CERCETĂRII TINERETULUI ŞI SPORTULUI
OIPOSDRU
UNIVERSITATEA BABEŞ-BOLYAI CLUJ-NAPOCA

Jury

President: Conf. uni. dr. Cornelia Majdik	Babes-Bolyai University
Scientific advisor: Prof. dr. Mircea V. Diudea	Babes-Bolyai University
1. Reviewer: Prof. dr. Bazil Pârv	Babes-Bolyai University, Faculty of Mathematics and Computer Science
2. Reviewer: Conf. uni. ing. dr. Mihai Medeleanu	Polytechnic University of Timisoara, Faculty of Industrial Chemistry and Environmental Engineering
3. Reviewer: Conf. uni. dr. Ionel Humelnicu	Alexandru Ioan Cuza University, Faculty of Chemistry

Table of contents (as in the full text) Page

Key terms: *fullerene, isolated pentagon rule (IPR), pentagon adjacency penalty rule (PAPR), highly ordered pyrolytic graphite (HOPG), surface enhanced Raman spectroscopy (SERS), Raman spectroscopy, IR Spectroscopy, density functional theory (DFT), crystal-like network, Omega polynomial.*

Introduction

The carbon materials have drawn attention both to science and also to technology due to their unique physical and chemical properties. The fullerene structure (C_{60}) discovered in 1985 wear the name of the well-known American architect Buckminster Fuller, who invented the geodesic dome. The discovery of fullerenes and their recognition by awarding the Nobel Prize for Chemistry in 1996 opened the doors to new research. Another class of compounds related to fullerenes are the carbon nanotubes, discovered after 1991 by the Japanese Sumio Iijima. In 2004 graphene was discovered through graphite exfoliation; it has some special properties which confer it an extraordinary potential, both for theoretical physics and for making new applications. In 2010 two researchers, Andrei Geim and Konstantin Novoselov were awarded the Nobel Prize for Physics for their revolutionary work on graphene. The graphene is the bidimensional variant of graphite which is made of a hexagonal net.

These series of prizes prove the importance of the new carbon structures for fundamental physics studies and also for the future of nanotechnology. The exploitation of the unique properties of carbon nanostructures in new high performance devices, like transistors, should be expected. Recently a new research has seemed to help to separate these nanostructures, namely theoretical predictions of new carbon structures joined by experimental measurements which try to isolate the stable carbon structures or to develop blocks of periodical materials made up of carbon atoms. New periodical materials of carbon have been theoretically predicted through the application of more cyclic transformations of the carbon structures and also their conversion in stable macroscopic nets. This combination seems to be the most promising to find new carbon structures. From the experimental point of view there are many groups who work to obtain carbon materials applying different procedures.

Very recently, a new procedure to obtain the carbon materials deposited on an underlayer of highly ordered pyrolytic graphite (HOPG) was obtained in 2006 by A. Böttcher and collaborators namely through electronic impact, followed by fragmentations of large fullerenes (for example C_{60}), and obtained successfully cages of smaller dimensions (for example C_{58}). This method converses the stable fullerenes IPR (IPR: the rule of isolated pentagon) in smaller carbon non-IPR cages, these representing different structural units, for example two adjacent pentagons. Motivated by the recent research progress regarding the carbon nanostructures, we decided to do extended theoretical work, namely the prediction of the geometry of the small fullerene cage and also the description of blocks of periodical materials made of carbon atoms.

The Ph D Thesis is structured in four chapters:

Chapter 1. *IPR and non-IPR Fullerenes*, where basic terms and concepts are explained, being important for investigation of fullerenes.

Chapter 2. *DFT Calculations for fullerenes*, where calculations of density functional theory (DFT) are presented. The Turbomole programme, version 6.2 is presented to identify the C_n cage geometry and also the vibronic properties of small fullerenes C_n ($n<70$). The small fullerene cages are considered to be in one of the following conditions: a) isolation of C_n cages one onto the other with the help of noble gases, b) C_n cages which form oligomers stabilised through covalent bonds which stabilise the non-IPR solid material. With the help of DFT calculations we can make the distinction not only between the electronic states of the C_n cages (neutral, cations and anions) but also the specification of the structure of the specific isomer. The density functional theory (DFT) predicted their structures and properties, which are also checked with experimental results obtained recently (Raman spectra and IR). The comparison helps us to understand some details that occur in the experimental part of the C_n solid material newly created. Nowadays the C_n solid materials can be made through perfect mass selection, but the control regarding the isomeric component remains a challenge. Thus, the main goal in the first part is to support the experimental part, namely the identification of possible isomers from the solid material newly created.

Chapter 3. *Topological description of the crystalline networks* in which operations on maps are presented; they were used to build basic units of new crystalline networks, these networks being topologically characterised using the Omega polynomial. The newly built networks present oriented cavities like those seen in zeolites which are largely used in chemical synthesis as catalysts.

Chapter 4. *Conclusions*, where general conclusions referring to Chapters 2 and 3 are presented.

The research in this area is interesting also from the perspective of finding new ways to identify the geometry of C_n fullerenes from the fullerenic material and also the description of crystalline networks that aim to simulate the canals occurring in zeolites.

2. DFT Calculations for fullerenes

In order to identify the geometry of C_n fullerenes from the fullerenic material obtained by the group headed by Prof. Dr. Manfred M. Kappes (Karlsruhe Institute of Technology (KIT)), we did calculations using the density functional theory (DFT), using the Turbomole programme. The aim of this study is to identify the geometry of the C_n cage dominant in the fullerenic material for this we did DFT calculations both for monomers and dimers, giving more attention to Raman and IR spectra.

2.1 Introduction

The calculations of density functional theory (DFT) can greatly help to determine the molecular structure, to explain the experimental spectra and also to calculate some physic-chemical parameters. While comparing the calculated spectra (IR and Raman) to those obtained by experiments, the most probable C_n cage can be identified. Moreover, it is expected to do the crystallographic structural solution at mesoscopic length scale, for example to find the local configuration of the most stable C_n cage.

The recent progress in Low-Energy Cluster Beam Deposition (LECBD) allowed to obtain new materials of great relevance in technology. Extending the classical cluster beam depositions setup by quadruple-based mass filtering and applying retarding potential in the collecting sample the soft-landing of mass-selected cluster ions became an efficient tool for fabrications of monodisperse materials. The potential of this technique demonstrated convincingly the increase of films with the help of selected mass of non-IPR fullerenes, C_n ($50<n<70$). In contrast to the well-known classical fullerenes C_{60} and C_{70} which satisfy the isolated pentagon rule (IPR), the „*non-IPR*" fullerenes are made up both of *IPR* and *non-IPR* units: adjacent pentagons (AP), squares and heptagons, etc.

The *non-IPR* C_n ($50<n<70$) fullerenes were generated by applying an induced electronic impact through the fragmentation of classical C_{60} and C_{70} fullerenes and this process takes place by sequential release of C_2 units.

$$\mathbf{C_{60} + e \rightarrow C_{58} + e + C_2 \rightarrow C_{56} + e + C_2 \rightarrow ...}$$

It was possible to create a new monodisperse fullerenic material through the extension of the „LECBD- Low-Energy Cluster Beam Deposition" technique meaning to make a mass selection of the molecular mass units requested, for example C_{58} with the mass m=696. However, the procedure does not provide a reliable control of the atomic structure of the cage. The final structure of a C_n isomer is the result of a cascade fragmentation process:

$$\mathbf{C_{60} \rightarrow C_{58} \rightarrow C_{56} \rightarrow C_{54} \ldots,}$$

This stage is governed by the following stages as: induction of electronic impact, vibrational excitations, ionisation and detachment of C_2 units. Despite the complexity of cascade generation, the tendency to get to the cage structure of the most stable non-IPR conformers was demonstrated.

The calculations that were done using the DFT method, in the case of small isolated C_n cages, help to elucidate the atomic structure of the most stable isomers. It was proved that the most stable isomers of non-IPR structural motifs, mostly 2AP, 3AP and Hp as localized reactions centers present increased abilities to form bonds between cages.

2.2 Vibrational Analysis of Fullerenes

This part consists of a comparison between experimental spectra and simulated Raman and IR spectra, calculated with the help of the density functional theory (DFT), using Turbomole software.

2.2.1 Computational Details

In order to identify the dominant isomers in the fullerene material, we performed computations with the help of the DFT method for monomers and dimmers as well, focusing upon Raman and IR spectra. The initial geometry of the fullerenes was obtained with the help of CaGe software. The newly obtained structures were initially pre-optimized with PM6 method, with the help of Mopac 2009 program. All the calculations were performed using the Turbomole software, followed by RI-DFT method (RI is the resolution regarding the exchange of functional and identity correlation), with the Becke-Perdew (BP86) functional, using two basic sets: *def-SV (P) and def2-SV(P)* to calculate the structure and vibrational spectrum. The wavelength that was used in the calculation of the Raman spectrum was 785 nm. In this paper we have developed a general

methodology that allows the elucidation of molecular structures of fullerene clusters, based on vibrational spectra acquired experimentally, and computations of the density functional theory (DFT).

2.2.2 IR Spectrum

In this part we present the simulated IR spectra of C_{60}, C_{60}^-, C_{60}^+ species compared to IR experimental spectrum accomplished by isolating the C_n cages with the help of noble gases.

2.2.1 IR Spectrum of C_{60}, C_{60}^-, C_{60}^+

In 1993 Maier and his collaborators published the IR spectrum of C_{60}^+ that we will use as it follows as a comparison between the experimental spectrum and the calculated one. With the help of the density functional theory (DFT) the systems can be simulated for a quality understanding of ions in a matrix of inert gas. The neutral molecules of C_{60} have four lines with high intensity in the thick films: at 526,5 cm^{-1} ($F_{1u}(1)$), 575, 8 cm^{-1} ($F_{1u}(2)$), 1182,9 cm^{-1} ($F_{1u}(3)$), 1429, 2 cm^{-1} ($F_{1u}(4)$) as well as many other lines of lower intensity $F_{1u}(1)$ and $F_{1u}(2)$ that represent the radial vibrations of the two cages of deformed fullerene. The most intense vibrations are at $F_{1u}(3)$ and $F_{1u}(4)$, this peaks are features for the pentagon, in an unaltered cage. In the figure below we see the IR spectrum of C_{60}^-, C_{60}^+ species and C_{60} carried out by isolation in the matrix (green colour) and in the same spectrum we have represented the experimental spectrum reported by Maier as well as the calculated spectra of the following specie: C_{60}^-, C_{60}^+ and C_{60}. The calculated spectra for the neutral molecules, for cations and anions represented in figure 1 show high intensities of the absorption lines of the ions, due to electron-molecule vibrations (EMV).

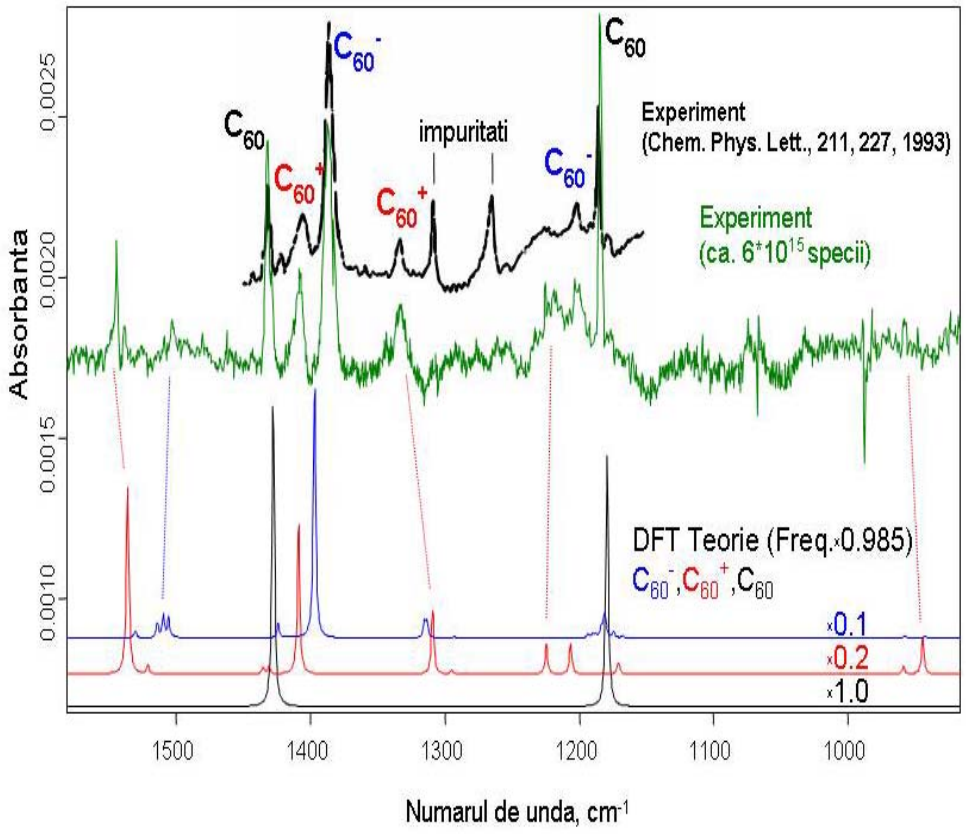

Figure 1. Comparison between the experimental IR spectrum (green) and C_{60}^- and C_{60}^+, C_{60} calculated spectra (blue, red and black). The intense black represents the literature IR spectrum.

Before the calculated frequencies were compared to the experimental ones, they were scaled as it follows: the intensities from the anionic and cationic spectrum were scaled with a 0,1 factor, respectively 0,2 and the intensities from the neutral spectrum were scaled with 0,2. These new absorption intensities are a better match with the experiment (Figure 1). Taking into consideration this shifting, as well as the correction of the intensity of the absorption lines, we can confirm the match with the experimental spectrum.

Analysing the IR spectrum we can acknowledge two absorption lines of low intensities at corresponding to C_{60}^-. By comparing the simulated spectrum with the experimental one, we can notice the line corresponding to C_{60}^+. The absorption lines from 1332 cm^{-1} from the simulated spectrum can be assigned to C_{60}^+ cation or C_{60}^- anion, both ions exhibiting in this area the same absorption line. Based on the theoretical calculations, the intensities of the absorption lines of C_{60}^+ can be noticed as well in the experimental spectrum as being dominant, and a contribution of this line for C_{60}^- cannot be taken into consideration.

With the help of simulated spectra we could identify the spectral lines of the existent species in the spectrum that was obtained experimentally. An analysis of the IR spectra, obtained experimentally of different C_{60} species is possible by assigning the absorption lines obtained through DFT calculation method.

2.2.3 Raman Spectra

In this part we compare Raman spectra obtained through DFT calculation method with the spectra experimentally obtained.

2.2.3.1 Fullerene C_{58}

The *non-IPR* C_{58} Fullerene were generated by enforcing an induced electronic impact by fragmenting the clasical C_{60} fullerene, and this process takes place by sending sequences of C_2 units. The final structure of a C_n izomer is the result of a cascade fragmentation process:

$$\mathbf{C_{60} \rightarrow C_{58} \rightarrow C_{56} \rightarrow C_{54} \ldots,}$$

This stage is rouled by the following steps: inducing the cascade impact; it was proven the tendency of reaching the cage structure of the most stabile non-IPR conformers.

Calculations made using DFT method, for small isolated C_n cages, help elucidate the atomic structure of the most stabile isomers. It was proven that the most stabile isomers of the non-IPR fullerene that contain in their sphere 2AP, 3AP and Hp units are reaction centers. These centres presented increased abilities of forming links between cages. In order to idenify the geometry of the fullerene isomers from the monodisperse material we started by generating C_{58} fullerene structures in CaGe programe. After this, these isomers were optimized with the help of PM6 method, using MOPAC 2009 program. The number of clasical and non-clasical C_{58} fullerene isomers is 23.995. they are formed of cicles of 5 and 6 and one cicle of 7. In this respesct we have taken into consideration the following C_{58} fullerene isomers with C_{3v} simetry, C_{58} with C_s simetry and C_{58} with C_2 simetry.

Table 1. Simetry, structure (name of the cycle, different isolated structures of isolated pentagon and hexagon) and number of adjacent pentagons.

Fullerene	Simetry	Structure
C_{58}	C_{3v} C_s C_2	3-2AP 2-C3AP+1-Hp 2- C3AP

The optimized structures of these isomers are presented in the figure below:

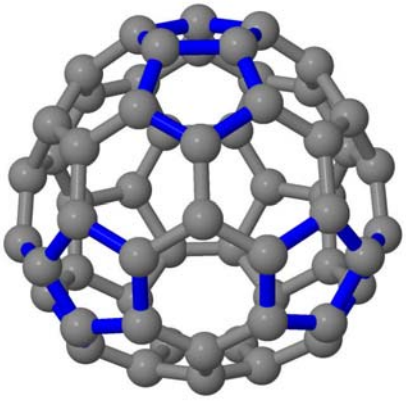

C_{58} (C_{3v}) (3-2AP)

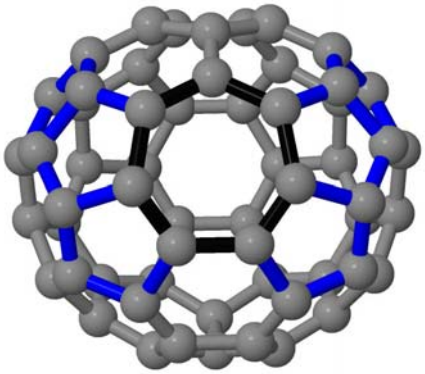

C_{58} (C_s) (2-C3AP + 1-Hp)

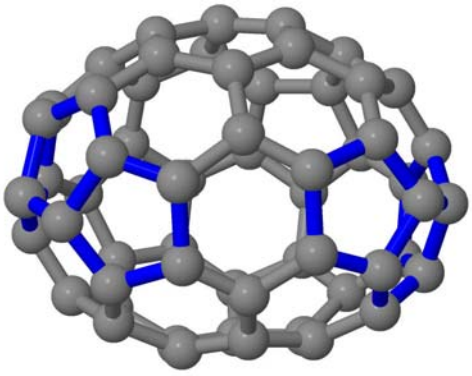

C_{58} (C_2) (2-C3AP)

Figure 2. Representation of the most stabile three isomers of C_{58} fullerene, which are the C_{3v} simetry isomer (left), C_s isomer (right), C_2 simetry isomer (midle).

Starting from the three monomers of C_{58} fullerene, C_{58}-C_{58} dimers were carried out, and we considered the cycloaddition process [2+2]. In the below figure we present the units that bind the clasical and non-clasical cages of IPR and non-IPR fullerene.

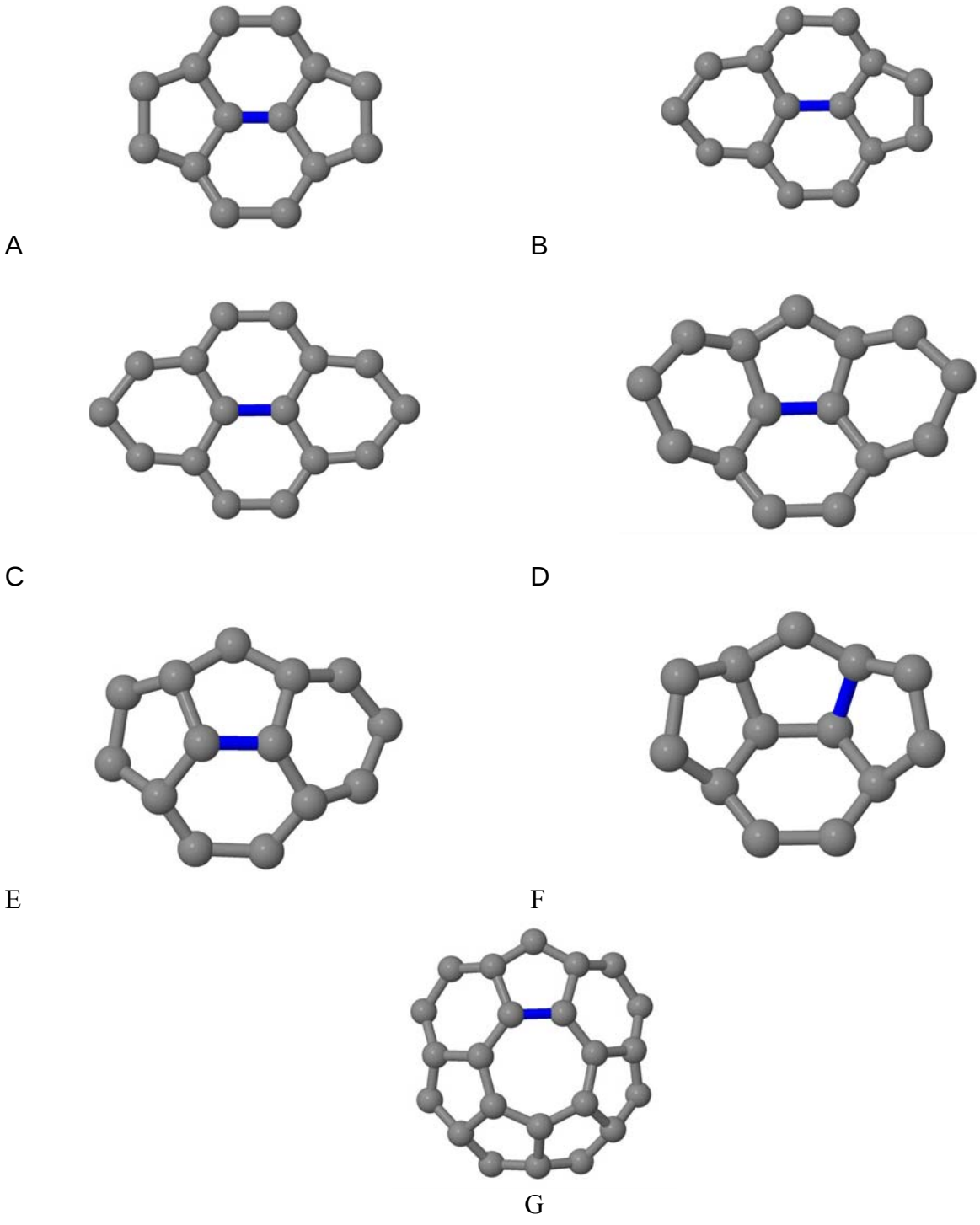

Figure 3. Units taken into consideration for the links between clasical and non-clasical cages of the IPR and non-IPR fullerene.

In figure 3 we presented the units taken into consideration for the links between clasical and non-clasical cages of the fullerene. The links between (non-IPR)-(non-IPR) were considered capabile of achieveing strong links between cages.

For each newely built dimer, with the help of Turbomole (RI/DFT def-SV(P)) programe, we obtained vibrational spectra. As it follows we compare the Raman spectra of C_{58} fullerene deposited on a surface of pyrolytic graphite with high orientation (HOPG) carried out by S. Ulas and his colaborators with the Raman spectra of the newly built dimers. As it followes we will assume that the vibronic propreties of the ologomers that form fullerene films could be described with the help of C_n-C_n dimers (calculating the long oligomers is considered too expensive). This strategy is rezonable in order to recognise the relation between theory and experiment.

In order to rebuilt the spectra obtained experimentally we created a number of models starting from the C_{58} (C_{3v}) and C_{58} (C_s) monomer. In the figure below we represented dimers that were built starting from the C_{58} monomers with C_{3v} and C_s simetry. These dimers are different by the unity in binding the cages. For the C_{58} isomer with C_{3v} simetry we took into consideration the following units in binding the cages: 55-55 and 66-66. As far as the C_{58} isomer goes, with C_s simetry, dimers were built with the following units: 56-55 si 57-56.

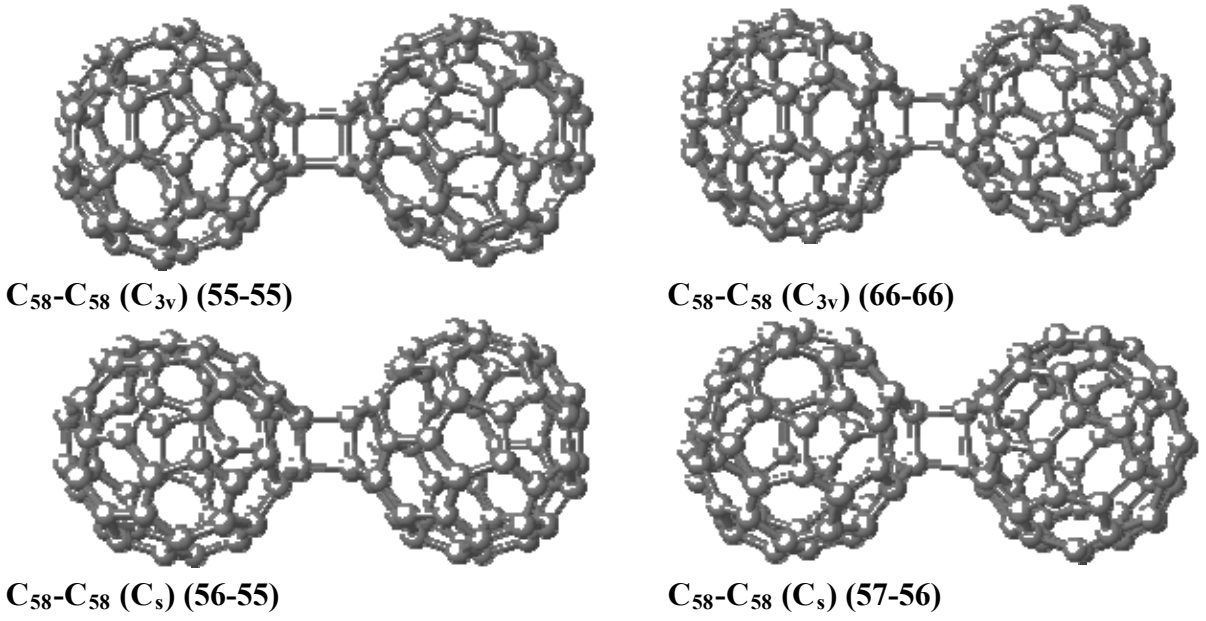

Figure 4. Optimized structures of C_{58}-C_{58} dimers startimg from the C_{3v} și C_s simetry monomers

We present in the figure above the ways of binding the dimers (for example: 55-55, represents the link between pentagon-pentagon) as well as the simetry of the monomers we started

with in forming dimers. For each newely built dimer with the help of Turbomole (RI/DFT def-SV(P)) program, we obtained vibrational spectra.

As it followes we represent the simulated Raman spectra of the four structures considered patterns in identifying the vibrational modes of the simulated spectrum, obtained by depositing it on a substrate of pyrolytic graphite with high orientation (HOPG).

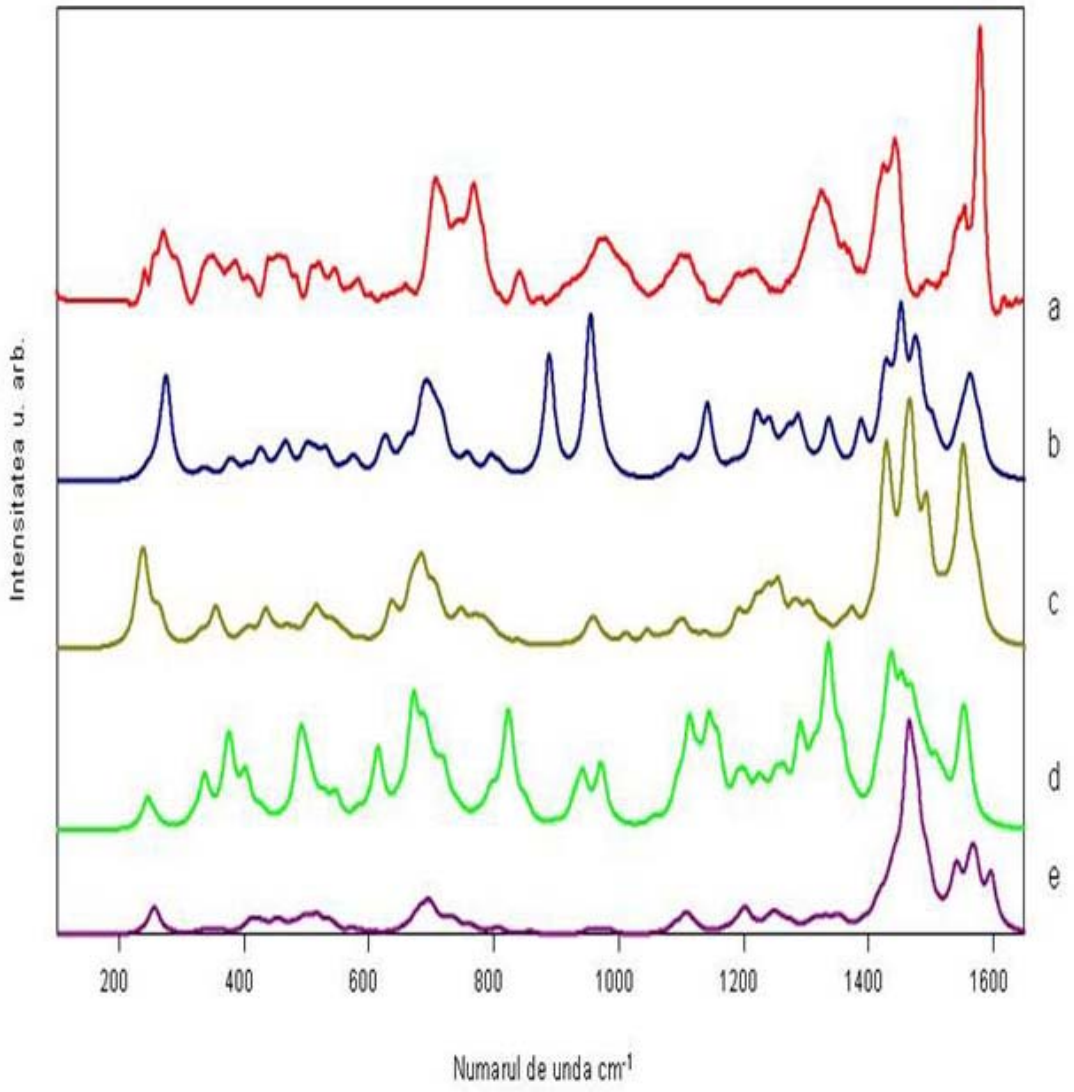

Figure 5. a) Raman experimental spectrum C_{58} HOPG (thick films), b) Raman simulated spectrum C_{58}-C_{58} (C_{3v}) (55-55), c) Raman spectrum C_{58}-C_{58} (Cs) (57-56), d) Raman spectrum C_{58}-C_{58} (C_{3v}) (66-66), e) Raman simulated spectrum C_{58}-C_{58} (Cs) (56-55).

The deposited films in the circumstances described above were studied through Raman spectroscopy, with a wavelength excitation of 785 nm, in order to observe the ordered faze in the

material. Camparing these spectra we expect to find bands that could correspond with C_{58} spectrum deposited on a surface of pyrolytic graphite with high orientation (HOPG), in order to identify the film's geometry.

Comparing the simulated spectra with the experimental spectra we notice that there are two intervals between 600-700 cm^{-1} where we see vibrational modes of medium intensities. In the interval 1390-1600 cm^{-1} we see vibrational modes of higher intensities. To note the fact that there are differences between the Raman simulated spectra. This proves that there are influences that start with different isomers with different links between the monomers. This makes us believe that in the fullerenic material we have other isomers with other types of starting geometries

The vibrational modes from the experimental spectrum could not be completly identified with the vibrational modes of the four dimers that were taken into consideration. The next isomer with the lowerst energy is C_{58} with C_2 simetry, that was used further in building dimers. The dimerization proccess was considered [2+2] and the units taken into consideration in binding the two cages are presented above (figure 3).

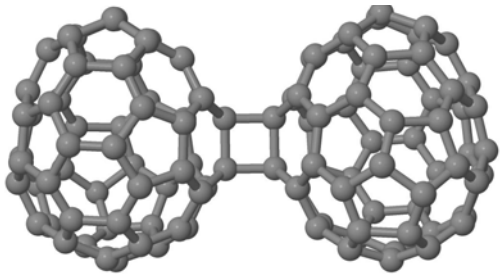

C_{58}-C_{58} A

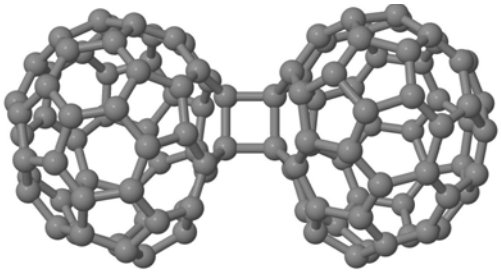

C_{58}-C_{58} B

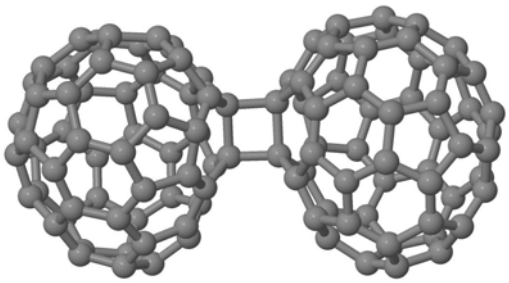

C_{58}-C_{58} C

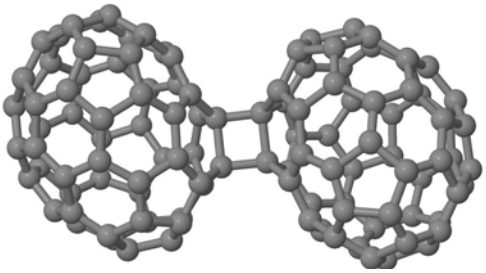

C_{58}-C_{58} D

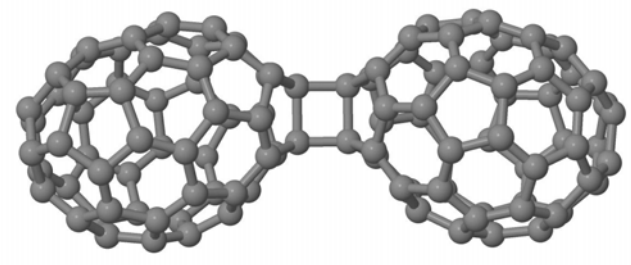

C_{58}-C_{58} E

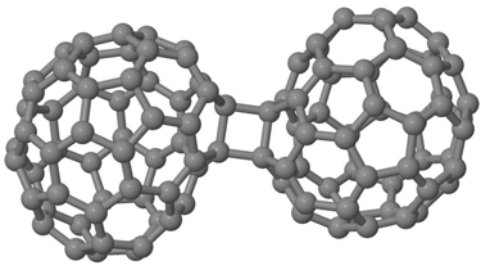

C_{58}-C_{58} F

Figure 6. Optimized structure of C_{58}-C_{58} dimers starting from the C_2, simetrie monomer with diferent binding.

For all the suggested models we calculated the vibrational spectra and as it follows they are compared to C_{58} spectra obtained on a layer of pyrolytic graphite with high orientation (HOPG).

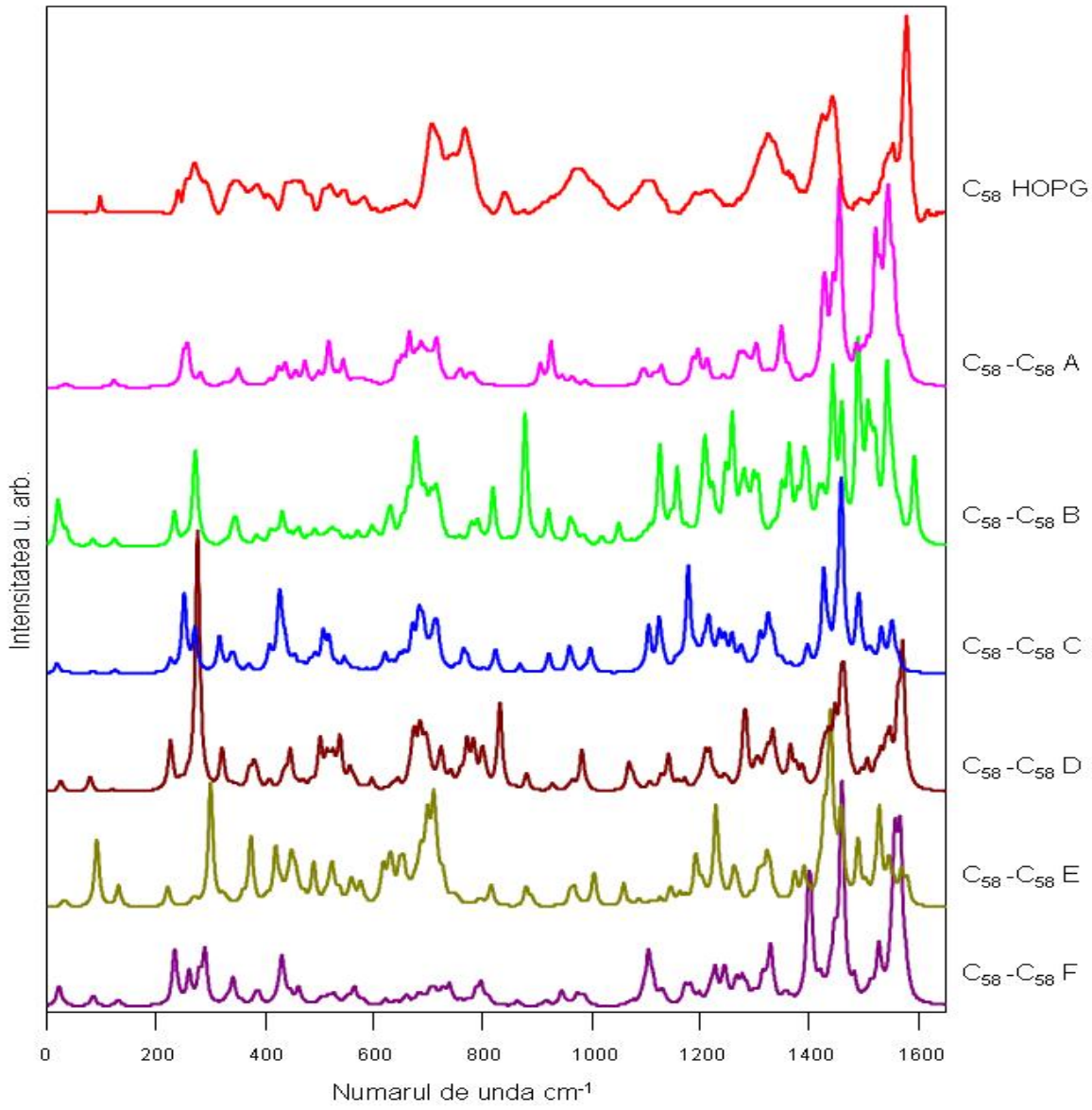

Figure 7. Raman experimental spectrum of C_{58} (thick film) layed on HOPG surface compared to the Raman simulated spectra for the following models that were taken into cosideration: C_{58}-C_{58} A, C_{58}-C_{58} B, C_{58}-C_{58} C, C_{58}-C_{58} C, C_{58}-C_{58} D, C_{58}-C_{58} E, C_{58}-C_{58} F.

C_{58}-C_{58} A, C_{58}-C_{58} B, C_{58}-C_{58} C, C_{58}-C_{58} C, C_{58}-C_{58} D, C_{58}-C_{58} E, C_{58}-C_{58} F simulated spectra do not fully reproduce the vibrational modes of the experimental spectra obtained on a HOPG surface.

2.2.3.2 Oxidation of film C_{60}

More calculations were done using the density functional theory (DFT), with the BP86 functional and with the basic set def-SV(P), for more molecular structures like $C_{60}O_n$ and C_{60}-O-C_{60} and the expectations are to find some qualitative modification seen in the vibrational spectra of the C_{60} oxides. Experimentally, the oxidation of C_{60} films was done in ultra high vacuum conditions, and these C_{60} molecules are stabilized through van der Waals bonds. Due to the kinetic energy obstacle at the room temperature, the oxides formation gets ~ 3 MLE. The strata that constantly result from $C_{60}O_n$, and also multi-cage aggregates stabilised by oxygen atoms interconnected contiguously between the cages of C_{60}, -C_{60}-, O-C_{60}. Instead, the thermal demounting of the film takes place through the simultaneous desorption of CO, CO_2, O_2 and C_{60}. The fullerenic material newly obtained was studied through UPS, XPS, Raman, TDS and AFM.

This study proves that adopting oxygen of C_{60} fullerene reduces significantly the molecule symmetry and the vibrational modes Hg and Ag are reduced, thing that constitutes the spectrum of the pristine C_{60}. In the figure below the structural models are presented, considered for the identification of Raman experimental spectrum.

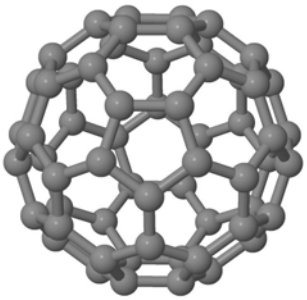

C_{60}

$C_{60}O$

$C_{60}O_5$

$C_{120}O$

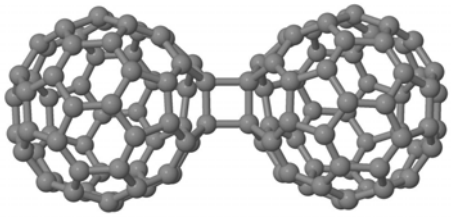

C_{120}

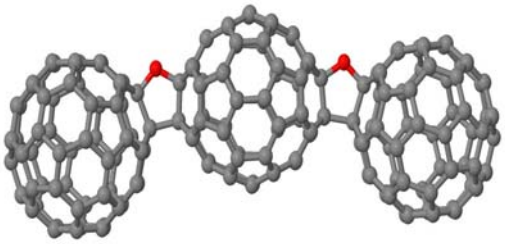

$C_{180}O_2$

Figure 8. The optimized structures of C_{60}, $C_{60}O$, $C_{60}O_5$, C_{120}, $C_{120}O$, $C_{180}O_2$.

In order to help to identify the spectral lines of the existing species in the Raman spectrum that was experimentally obtained of the oxygenation of films C_{60}, we calculated for the structured models that were considered (C_{60}, $C_{60}O$, $C_{60}O_5$, C_{120}, $C_{120}O$, $C_{180}O_2$) the vibrational spectra at the wavelength of 785 nm. Comparing the spectrum of the C_{60} fullerene to the other structural models ($C_{60}O$, $C_{60}O_5$, C_{120}, $C_{120}O$, $C_{180}O_2$) we can notice the reduction of the intensity of vibrational

modes in the range of 200-600 cm^{-1}. The strong vibrational modes Hg(1), Ag(1) and Hg(3) were replaced with many other vibration due to the oxygen. In the case of C_{60} fullerene oxidation the vibrational modes Ag(2) and Hg(8) are incongruous.

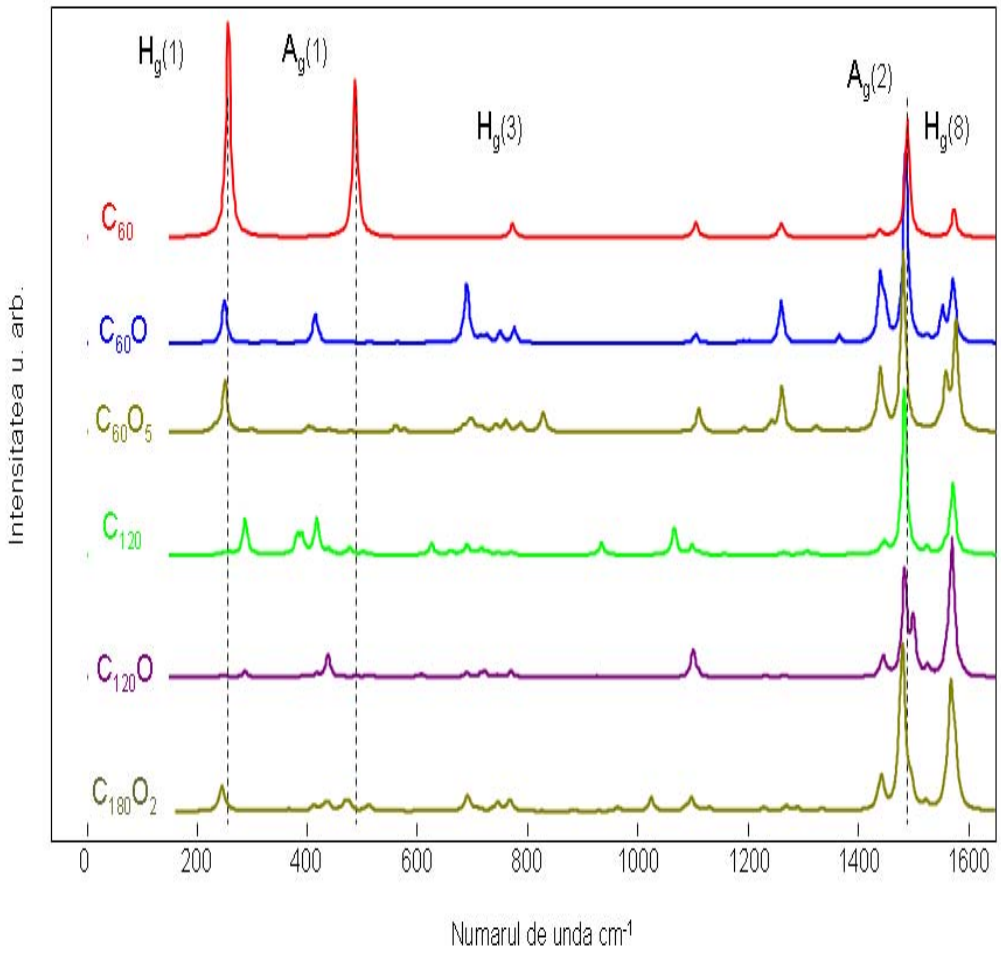

Figure 9. Simulated Raman spectrum of C_{60}, $C_{60}O$, $C_{60}O_5$, dimer C_{60}-C_{60}, complex C_{60}-O-C_{60} and C_{60}-O-C_{60}-O-C_{60}.

Comparing the simulated spectra to the experimental ones we can notice that there are two intervals between 200-700 cm^{-1} where vibrational modes with medium intensities occur, while in the interval 1400-1600 cm^{-1} vibrational modes with higher intensities occur for the considered structural models $C_{60}O$, $C_{60}O_5$, dimer C_{60}-C_{60}, complex C_{60}-O-C_{60} and C_{60}-O-C_{60}-O-C_{60}. In the figure below are compared the spectra the sum of simulated spectra with Raman spectra of the oxidised complex of C_{60} (black line) obtained through experiment and with the less intense black line is represented the experimental spectrum of C_{60}.

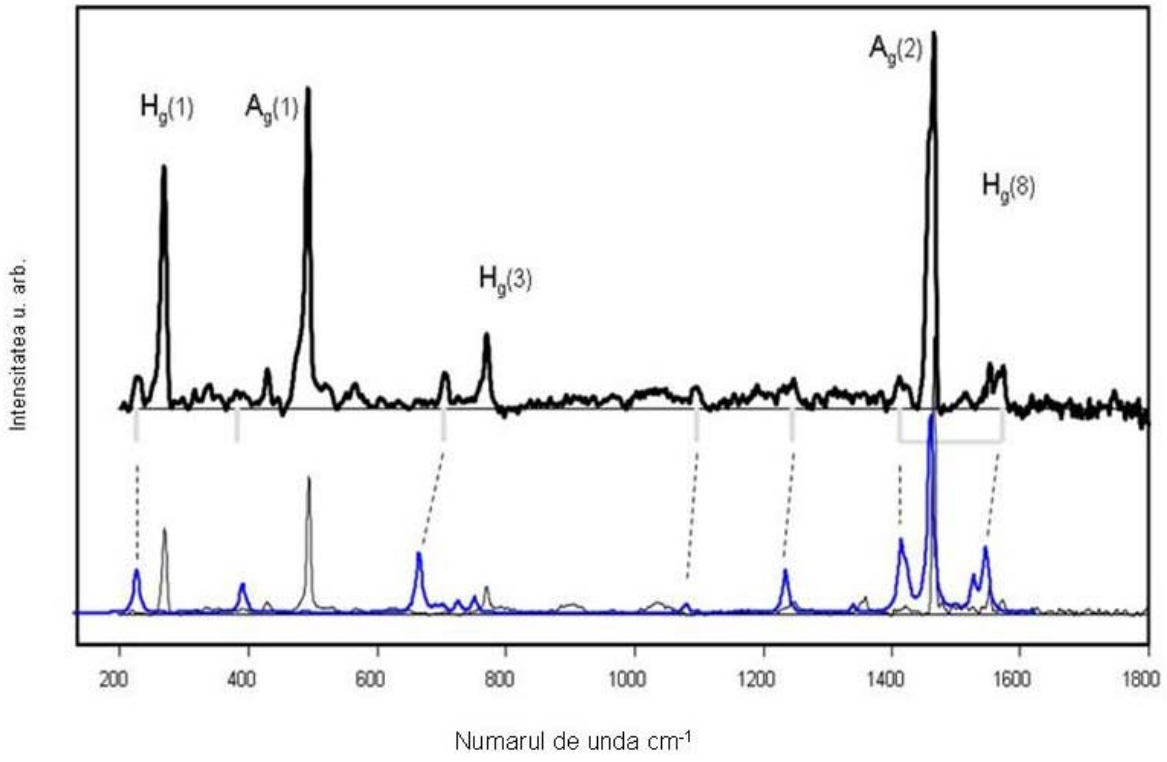

Figure 10. The representation of the Raman spectrum of the oxidised complex of C_{60} (black line) obtained through experiment and with the less intense black line is represented the experimental spectrum of C_{60} (thin films), while with the blue line is the sum of the calculated spectra of C_{60}, $C_{60}O$, $C_{60}O_5$, dimer C_{60}-C_{60} complex C_{60}-O-C_{60} and C_{60}-O-C_{60}-O-C_{60}.

It is surprising that the oxidised spectrum of film C_{60} is dominated by strong spectral features that are characteristic for clean spectrum C_{60} (thin films). All the Hg and Ag modes outlast the oxidation procedure. Comparing the simulated spectrum to the experimentally obtained spectrum of the complex C_{60} some modifications occur, which are marked with the grey line. However, we found a unique feature of derivative product which can see in the spectrum below.

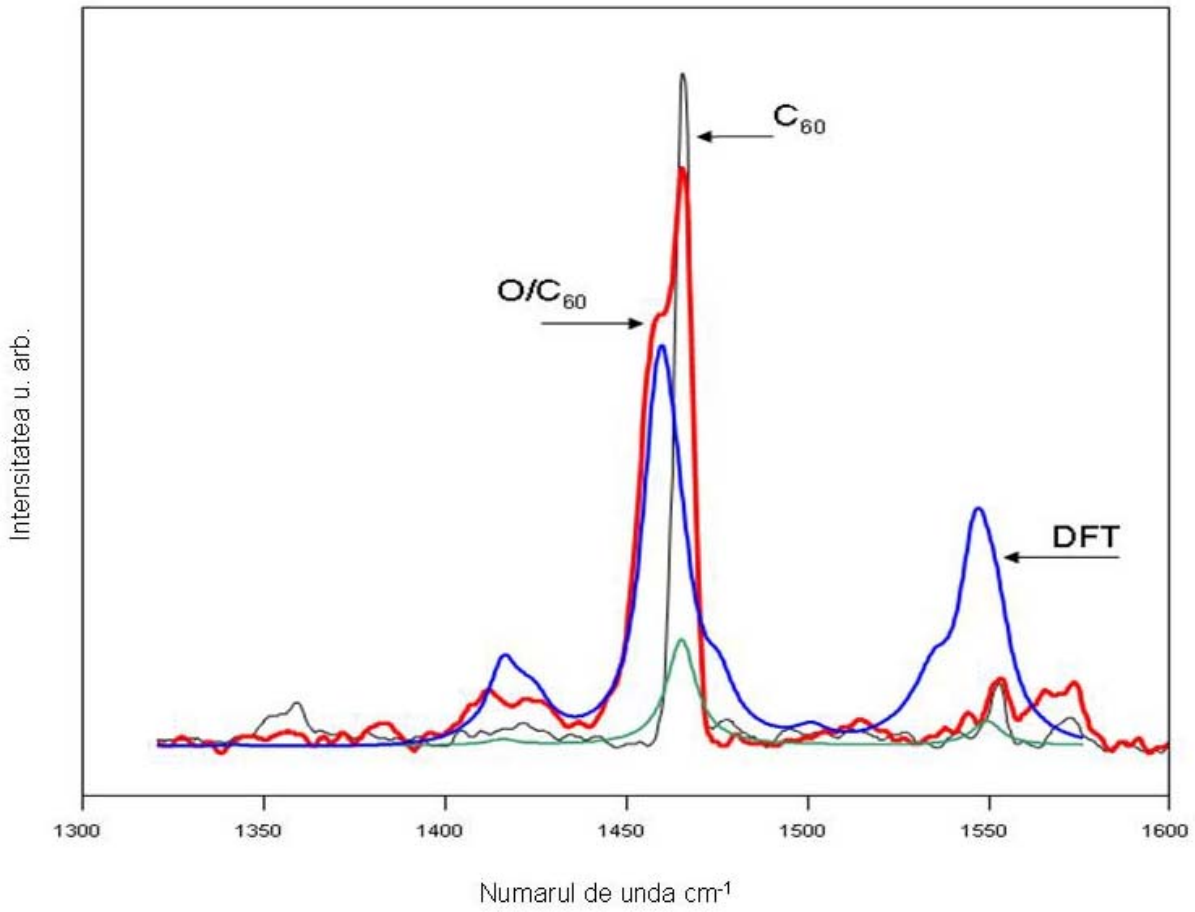

Figure 11. The graph representation of Raman spectrum in the 1300-1600 cm^{-1} interval of the experimental spectrum $C_{60}O$ (red), the experimental spectrum C_{60} (black) and also the simulated spectrum representing the sum of all the simulated Raman spectra obtained for C_{60}, $C_{60}O$, $C_{60}O_5$, dimer C_{60}-C_{60}, complex C_{60}-O-C_{60}, complex C_{60}-O-C_{60}-O-C_{60} (blue), and with the green line is represented the simulated Raman spectrum of C_{60}.

In the area 1300-1600 cm^{-1} in the experimental spectrum $C_{60}O$ (red) a new band occurs and it can be reproduced using the simulated spectrum namely through the sum of all the simulated Raman spectra for the considered models (C_{60}, $C_{60}O$, $C_{60}O_5$, dimer C_{60}-C_{60}, complex C_{60}-O-C_{60} and complex C_{60}-O-C_{60}-O-C_{60}), which illustrates an almost perfect reproduction with derivative number for centred Oxygen from 1458 cm^{-1}. Unfortunately from the experimental point of view, a more precise distinction of $C_{60}O_n$ and C_{60}-O-C_{60} has not been achieved due to the reduced sensibility of Raman spectrometer.

2.2.3.3 C_{60} Fullerene

Surface-enhanced Raman scattering (SERS) is a method to enhance the Raman intensity due to the interfacial phenomena of C_{60} films with the metal surface. In the case of C_{60} with high symmetry, it is possible to attribute the basic vibrational frequencies namely the active Raman modes. The theoretical computations were done with Turbomole software, version 6.2 (2010), that was followed by RI-DFT method (RI is the resolution regarding the change of identity functional correlation), with Becke-Perdew functional (BP86), using the basic set def-SV(P) to calculate the structure and the vibrational spectra**.** The wavelength that was used to calculate the Raman spectrum was of 785 nm, and the bandwidth is of 10 cm^{-1}. For a better interpretation of the SERS effect and to understand the interaction of C_{60} molecule with the SERS substrates (deposed on Klarite a substrate Au-SERS), we calculated the vibrational spectra of C_{60} molecule with a gold atom.

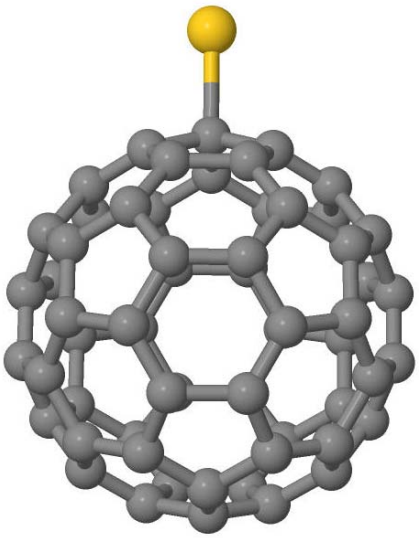

Figure 12. Molecule C_{60} Molecule with a gold atom.

The neutral molecules of C_{60} in the thick films present three lines of high intensity at 273 cm^{-1} (Hg(1)), 496 cm^{-1} (Ag(1)) and 1470 cm^{-1} (Ag(2)), and also many other lines of weaker intensities like: 709 cm^{-1} (Hg(3)) and 1575 cm^{-1} (Hg(8)).

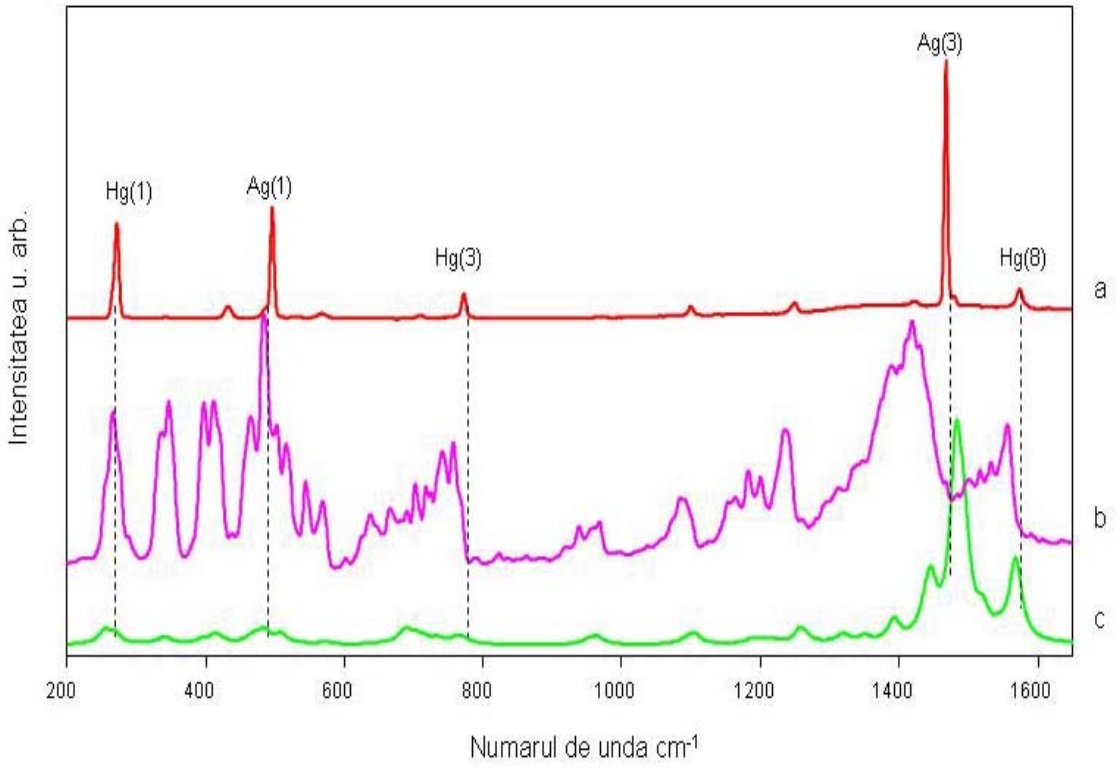

Figure 13. a) C_{60} experimental Raman spectrum (red), b) C_{60} SERS thin films (pink), c) simulated spectrum of $C_{60}Au$.

The spectral lines with higher intensities from the experimental spectrum match perfectly with the lines from the simulated spectrum, but in the experimental spectrum there occur spectral lines that are amplified by the electromagnetic field. Measuring the Raman spectrum of C_{60} fullerene (thin films) deposited on SERS substrates (deposed on Klarite a substrate Au-SERS), it has a different structure as seen in the spectrum from figure 13.

In the same time, with the help of calculation of quantic chemistry based on the density functional theory (DFT) were also calculated the wave numbers that match the vibration normal modes of the investigated $C_{60}Au$ molecule. When the C_{60} molecules are absorbed on a gold surface, the I_h symmetry of C_{60} molecule is reduced and the result is a fragmentation of Raman bands having also a degeneration of vibrational modes. The number of vibrational modes is increased in the SERS spectrum as seen in the figure below. When the C_{60} is absorbed on a gold surface through the pentagon, the molecule symmetry is reduced from I_h to C_{5v}. When the absorption takes place through a hexagon the symmetry is reduced from I_h to C_{3v}.

The experimental vibrational spectra SERS and C_{60} were correctly assigned and then they were compared to the spectra obtained after DFT computation. As it can be noticed from the figure below where the vibrational modes of C_{60} molecule with I_h symmetry were split in more vibrational modes, the most of Raman bands occur due to vibrational degeneration of the molecule and also to the symmetry reduction of the C_{60} fullerene due to the interaction with the gold surface.

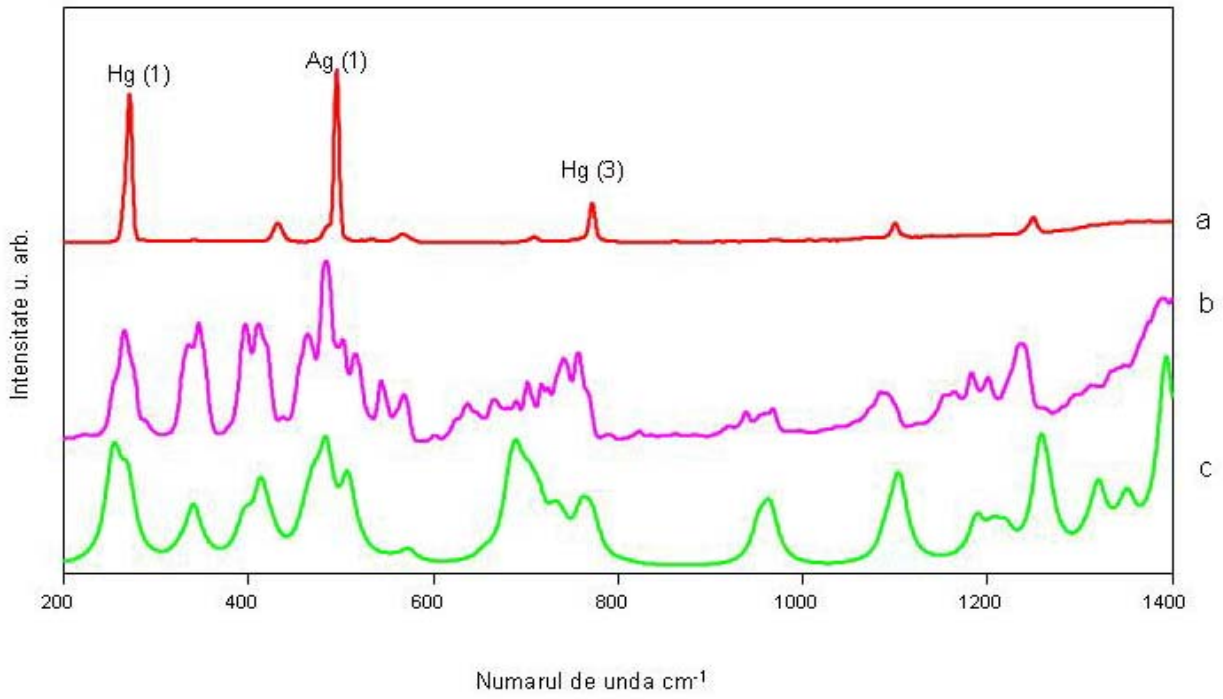

Figure 14. a) Experimental Raman spectrum C_{60} (red), b) SERS spectrum of C_{60} thin films (pink), c) simulated spectrum of $C_{60}Au$.

Due to the interaction with the SERS substrates, C_{60} molecule symmetry is reduced and the strong lines of the fullerenic film are suppressed while the weak modes are enhanced. Comparing the three Raman spectra (a, b, and c), more changes can be noticed in the bands and intensity positions, and in the range 200-1400 cm^{-1} there is a very good conformity between the SERS spectrum of C_{60} thin films (pink) and the simulated spectrum of C_{60} molecule with a gold atom.

2.2.3.4 C_{50} Fullerene

Fullerene C_{50} has 271 *classic isomers* and from these only two have lowest energies: the isomers with D_{5h} and D_3 symmetry. In each case they contain five or more pairs of contiguous pentagons distributed on the surface of fullerene. Also, C_{50} presents 2783 *non-classic isomers* which in turn contain other types of cycles like heptagons. According to semiempirical and quantum mechanics computations, it has been shown that classical isomers of fullerene C_{50} are, from energy point of view, more stable than non-classic isomers.

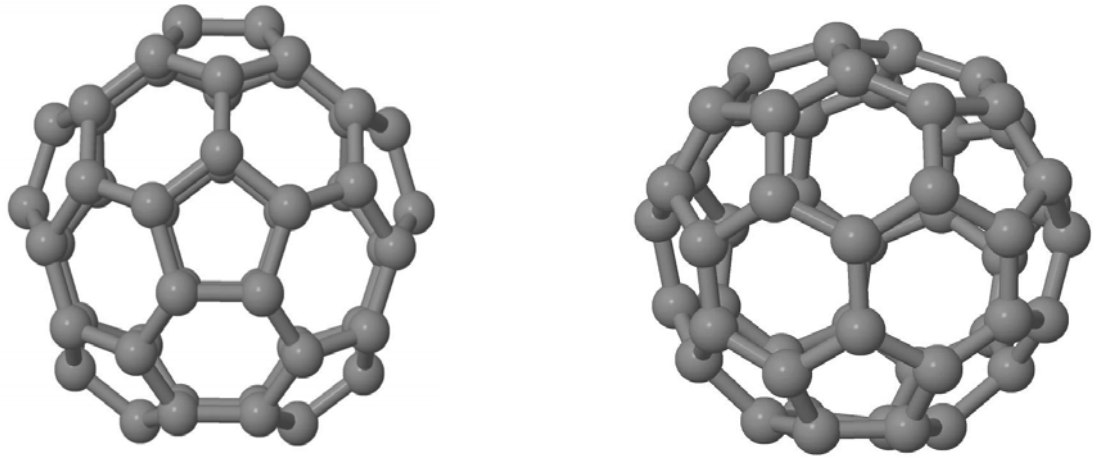

C_{50} D_{5h} (5-2AP) C_{50} D_3 (6-2AP)

Figure 15. Optimized structures of isomers C_{50} (D_{5h}) and C_{50} (D_3).

In the latest years the molecule $C_{50}Cl_{10}$ composed by 50 carbon atoms and stabilized by 10 chlorine atoms was synthesized, isolated, and characterized by Xie et al.

To reproduce the experimental SERS spectrum we have considered a few structural theoretical models used to identify the geometry of fullerene C_{50} from fullerenic material obtained. In order to identify the geometry of isomers from monodisperse films we created short oligomers C_n-C_n-C_n---C_n which are stabilized by covalent bonds e.g. between non-IPR positions of the two contiguous pentagons.

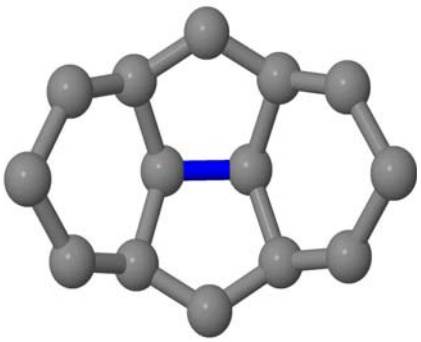

Figure 16. Structural unit considered for linking the two classic C_{50} cages.

Starting from the monomers of fullerene C_{50} with D_{5h} and D_3 symmetry we created dimers C_n-C_n, and the cycloaddition process was considered [2+2], the two fullerenes are bonded by two covalent bonds. Thus for the dimerization process of fullerene C_{50} we have considered the bonding between the two cages by pentagonal bonds.

Figure 17 shows the optimized structures of the dimer C_{50}-C_{50} starting from monomer C_{50} with D_{5h} symmetry, and the process of cycloaddition [2+2] was realized by pentagonal bonds. The same cycloaddition process was considered for the formation of dimer C_{50}-C_{50} but in this case we took into account the symmetric monomer D_3.

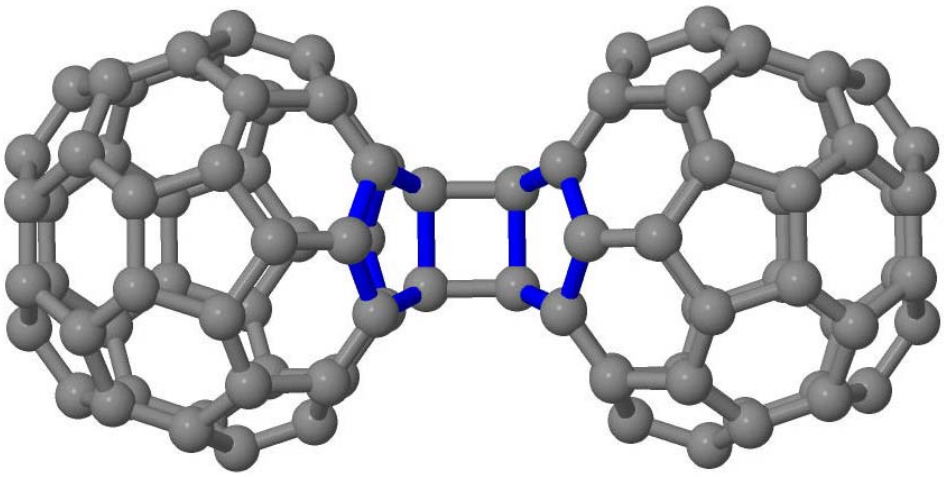

Figure. 17. Optimized structures of the dimer C_{50}-C_{50} with pentagonal bonds.

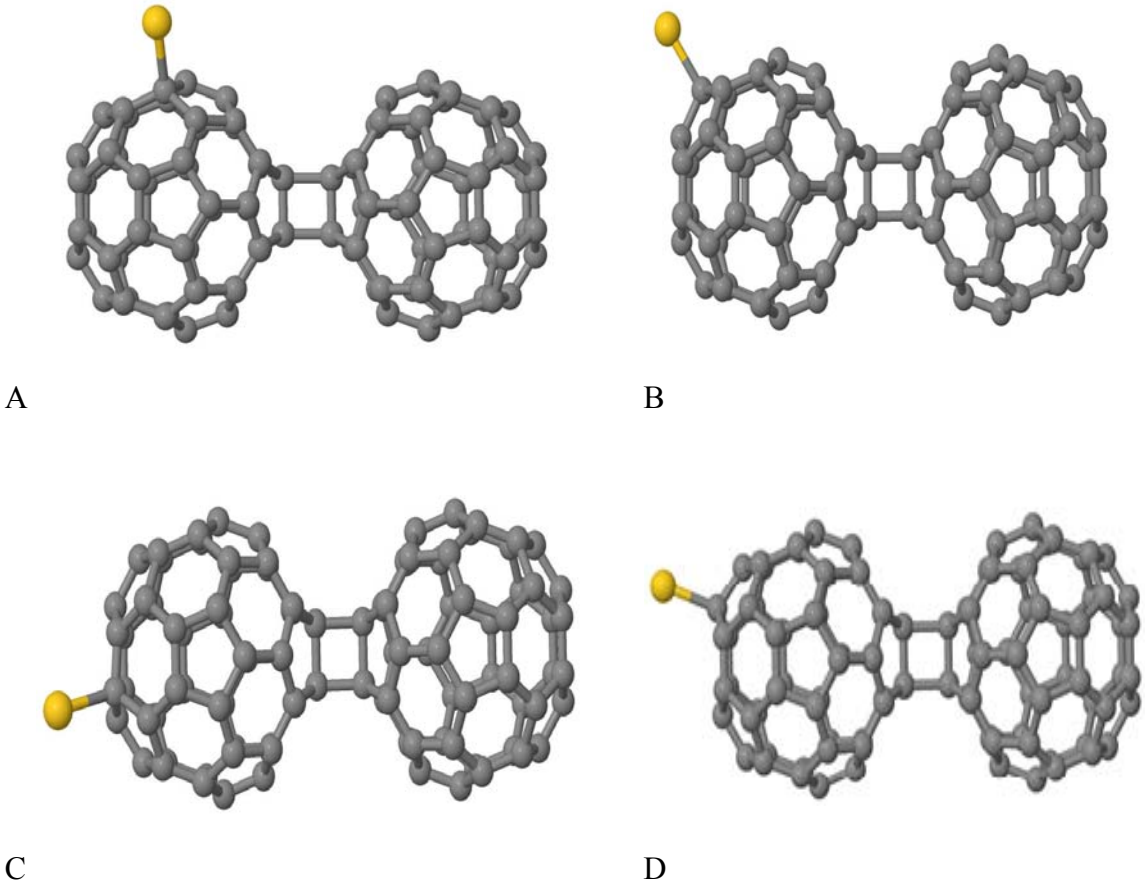

Figure 18. Different positions of the gold atom on the surface of the dimer $C_{50}(D_{5h})$-$C_{50}(D_{5h})$.

In order to help the characterization of the experimental spectra of fullerenes C_{50} from the fullerenic material deposited on SERS substrate (deposed on Klarite a substrate Au-SERS), we evaluated the vibrational frequencies of the dimers C_{50}-C_{50} with a gold atom. We created models starting from the same type of cycloaddition [2+2], using the same way to bond the dimer and by modifying the position of the gold atom on the dimer surface. Considering the high cost of these computations, the optimization geometry and vibrational models were obtained using DFT method with BP86 functional, basic set def2-SV(P), using Turbomole 6.2 software.

The figure below presents the C_{50}-C_{50} structures which were considered as models for explaining the SERS effect. To simulate the interaction of molecules C_{50} SERS thin films, we considered different positions of the gold atom bonded either by a pentagon or a hexagon.

Simulation of the Raman spectra of the fullerenic dimer C_{50}-C_{50}Au with different positions for the gold atom shows a match with the experimental spectra obtained on SERS substrate. The

following figure represents simulated Raman spectra for the four models (A, B, C, D) compared to the experimental spectra C_{50}.

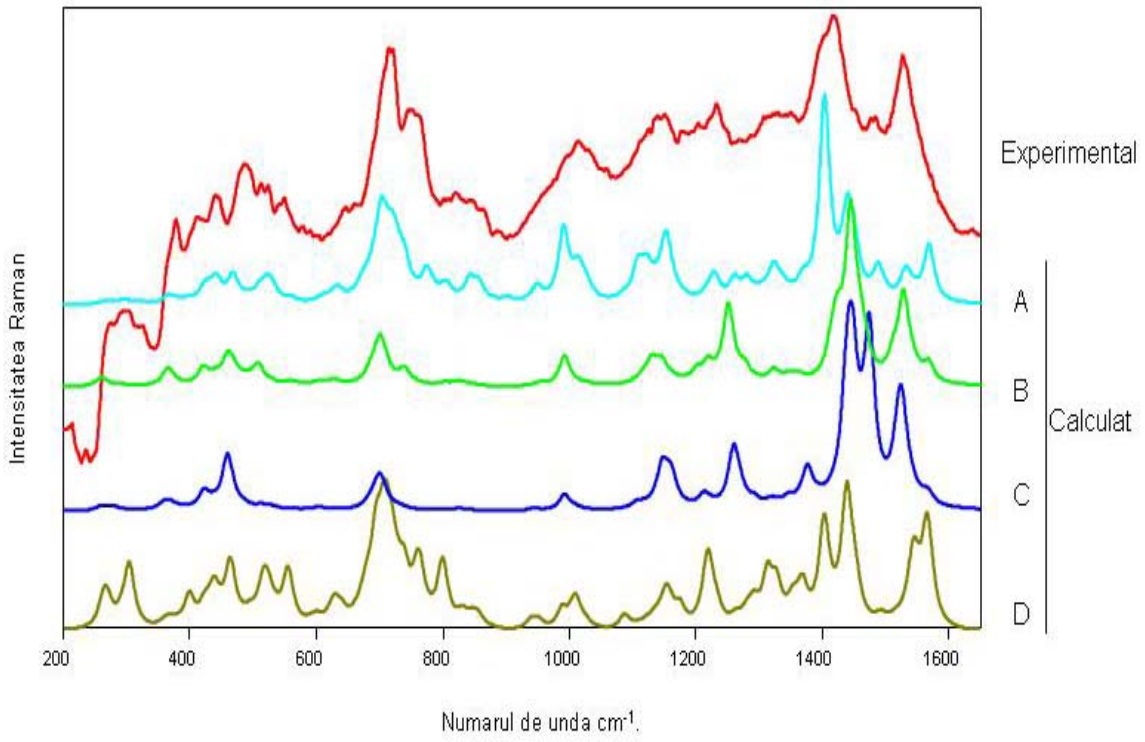

Figure 19. SERS spectra of the C_{50} film compared to these spectra of models C_{50}-C_{50}Au with different positions of the gold atom on the surface of fullerene.

As it can be observed, none of these simulated spectra totally explain the vibrational modes of the experimental spectra and in this case we considered a combination of these spectra, considering that one combination will better match the experiment.

In order to simulate the Raman spectrum of fullerene C_{50} caused by the interaction with SERS substrate we created different models starting from monomers C_{50} (D_{5h} and D_3 symmetry).

Due to the interaction with the SERS substrate, the molecule's symmetry is reduced and the strong lines of the film are suppressed and the weak modes are amplified. Strong interactions with electromagnetic field near the SERS substrate can be simulated by computing the C_{50}-C_{50} dimer with one gold atom.

In the figures below is presented the combination of structural models considered for the interpretation of SERS spectrum of the fullerenic material, namely:

a) The combination of A and B structures
b) The combination of C and D structures

In the figure below is presented the comparison of the simulated Raman spectrum with the spectrum of thick film of C_{50} deposited on a SERS substrate obtained experimentally. Then there is a comparison between the experimental C_{50} SERS spectrum and the sum of Raman spectrum of the models A and B and also the spectrum of dimer C_{50}-C_{50} (D_{5h}). When the two spectra are compared it is easy to notice that the simulated spectrum with the sum of Raman spectra of A and B models reproduces better the experimental spectrum.

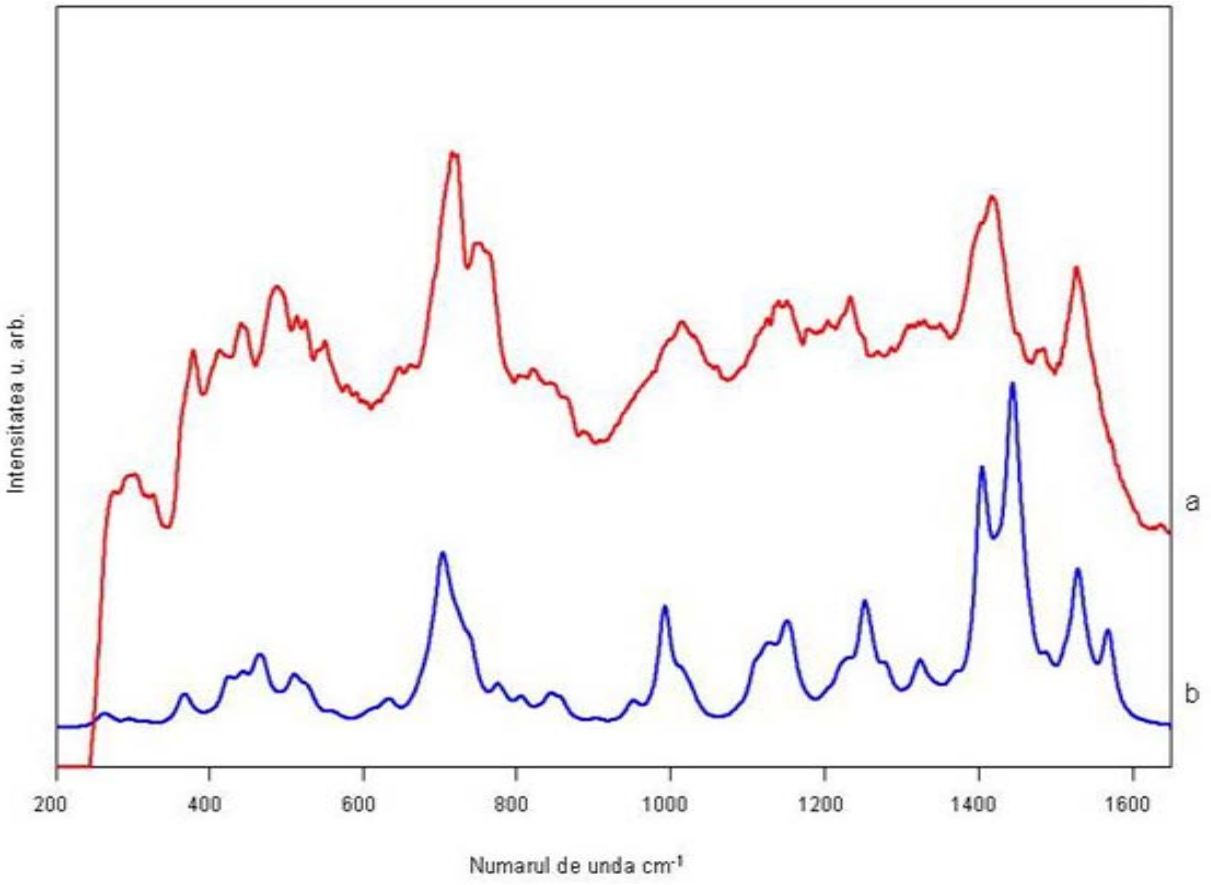

Figure 20. (a) The experimental SERS spectrum of film C_{50} and (b) the sum of simulated Raman spectrum of the structures C_{50}-C_{50} (D_{5h}) A and B.

In the spectrum below the combination of spectra models (C and D) is represented, starting from the same monomer in the dimer construction and what is different is the position of the gold atom on the fullerene surface. While comparing the experimental spectrum and the sum of spectra

of the two structures, the simulated spectrum does not replay completely the vibrational modes of the spectrum obtained experimentally.

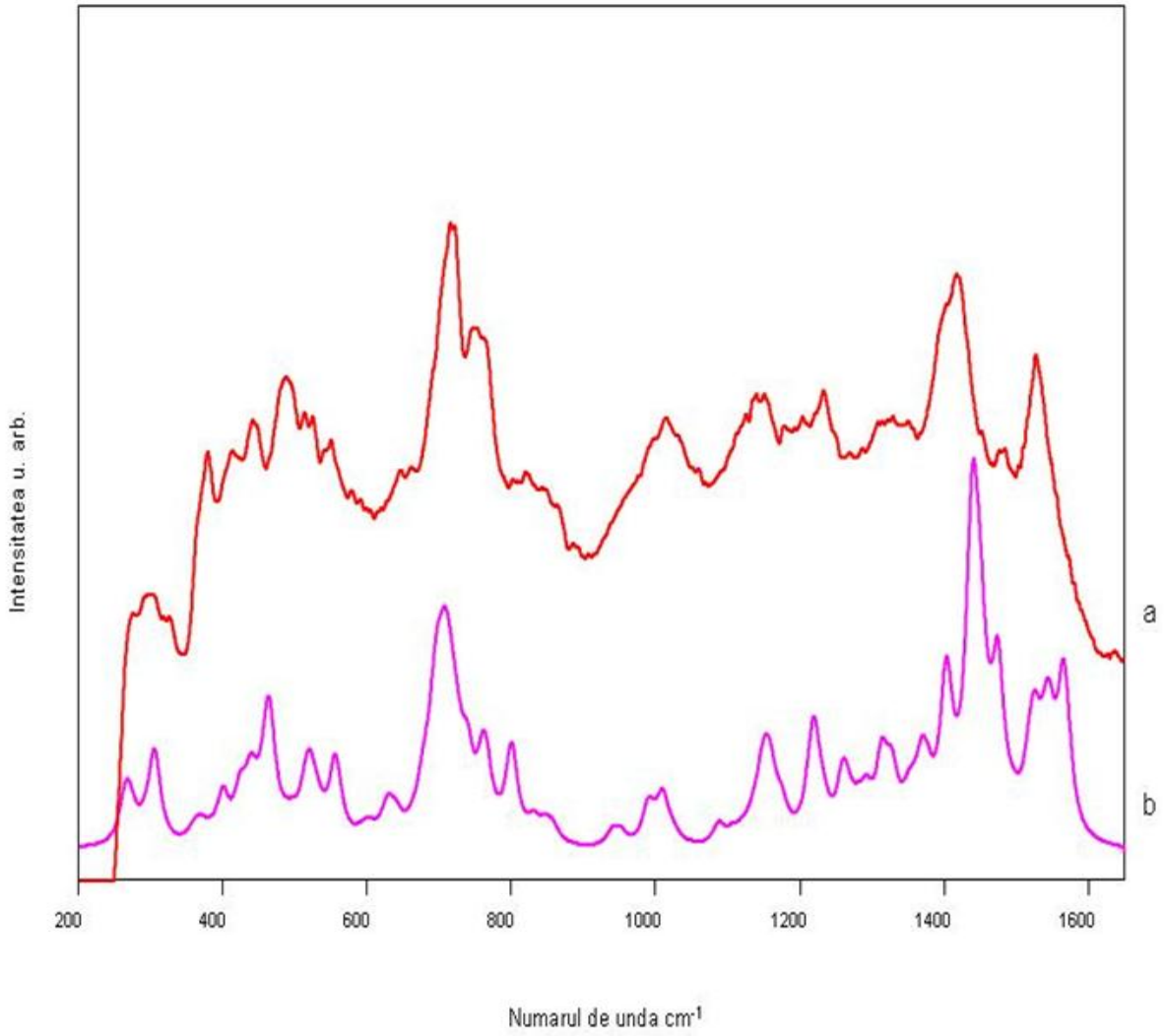

Figure 21. The experimental SERS spectrum of film C_{50} (red line) and the sum of simulated spectra of dimers structures C_{50}-C_{50} (D_{5h}) C and D (pink line).

We also compared the SERS spectrum of the film C_{50} (red line) obtained experimentally with the combination that reproduces better the experimental spectrum namely the sum of Raman spectrum of dimers C_{50}-C_{50} (D_{5h}) A and B and also the Raman spectrum of dimer C_{50}-C_{50} (D_{5h}).

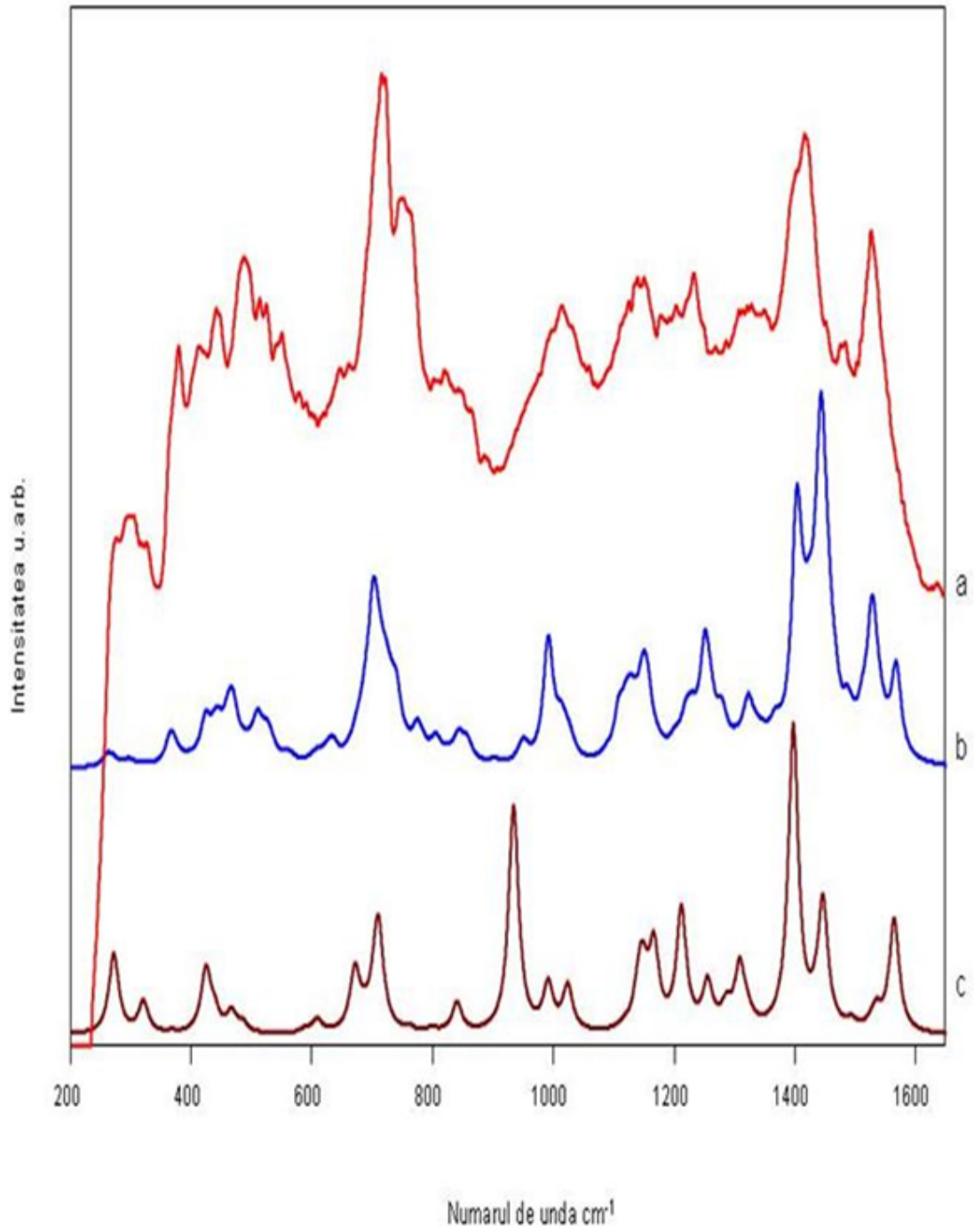

Figure 22. a) SERS experimental spectrum for C_{50} film, b) the sum of simulated spectrum of dimers structure C_{50}-C_{50} (D_{5h}) with different positions of the gold atom (A and B) c) simulated Raman spectrum of the dimer C_{50}-C_{50} (D_{5h}).

The Raman spectrum of C_{50}-C_{50} (D_{5h}) presents a common band in the interval 600-800 cm^{-1} with the Raman spectrum of dimers structure C_{50}-C_{50} (D_{5h}) with the different positions of the gold

atom (A and B) and also with the experimental SERS spectrum of the film C_{50}. Comparing the three spectra, the combination of the Raman spectrum of dimers structure C_{50}-C_{50} (D_{5h}) with the different positions of the gold atom (A and B) reproduces better the spectrum obtained through experiment. When the C_{50} molecules are absorbed on a gold surface, the symmetry of C_{50} molecule is reduced, and for this reason there is a fragmentation of Raman bands and also a degeneration of the vibrational modes. The number of the vibrational modes is higher in the SERS spectrum as it can be seen in the figure above.

We also built another type of structural models starting from the C_{50} monomer with D_3 symmetry and these dimers differ through the way the atoms of Au are disposed on the dimer surface.

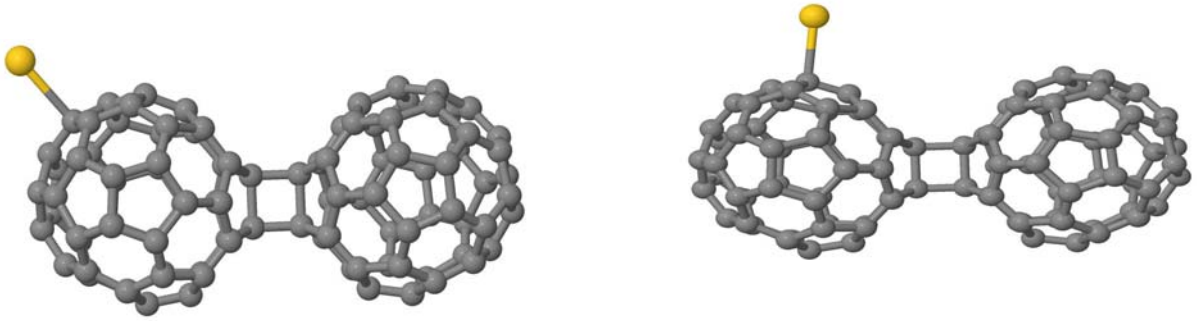

A B

Figure 23. Different positions of the gold atom on the dimer surface $C_{50}(D_3)$-$C_{50}(D_3)$.

Starting from the two structural models, the optimization geometry and the vibrational modes were obtained using the DFT method with the functional BP86, basic set def2-SV(P), using Turbomole 6.2 software. Then the simulated spectra were compared to the experimental spectra of the film of C_{50} (deposed on Klarite a substrate Au-SERS).

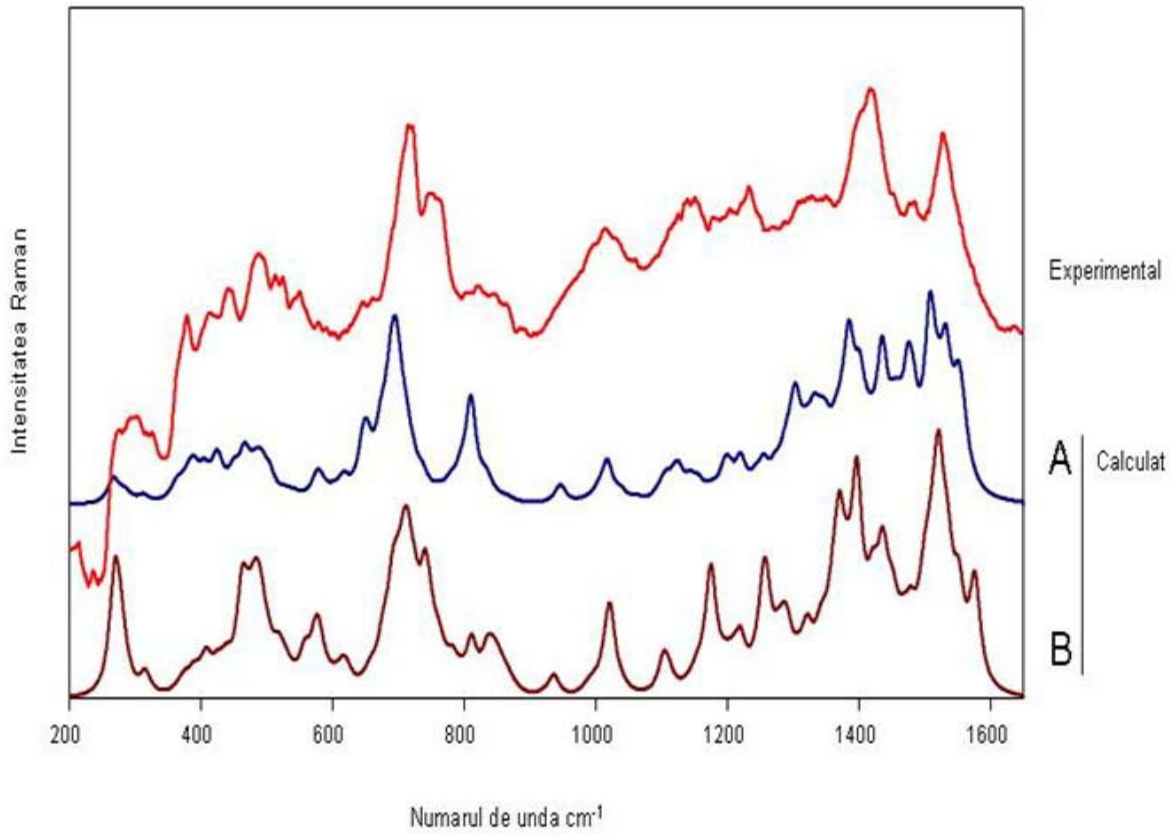

Figure 24. The SERS spectrum of the film C_{50} (red line) compared to the spectra of the models C_{50}-$C_{50}Au$ (D_3) with different positions of the gold atom on the fullerene surface.

Comparing the two SERS spectra and the Raman spectra of C_{50}-$C_{50}Au$ starting from the symmetrical monomer D_3, one can notice some difference. So, the most intense bands are those from 600-800 cm^{-1} and also the interval 1350-1600 cm^{-1}, and these vibrational modes obtained after doing calculations do not reproduce completely the vibrational modes from the experimental spectrum. I considered that the sum of spectra of the two structures with different positions of the gold atom, in the case of a better replay with the experimental spectrum.

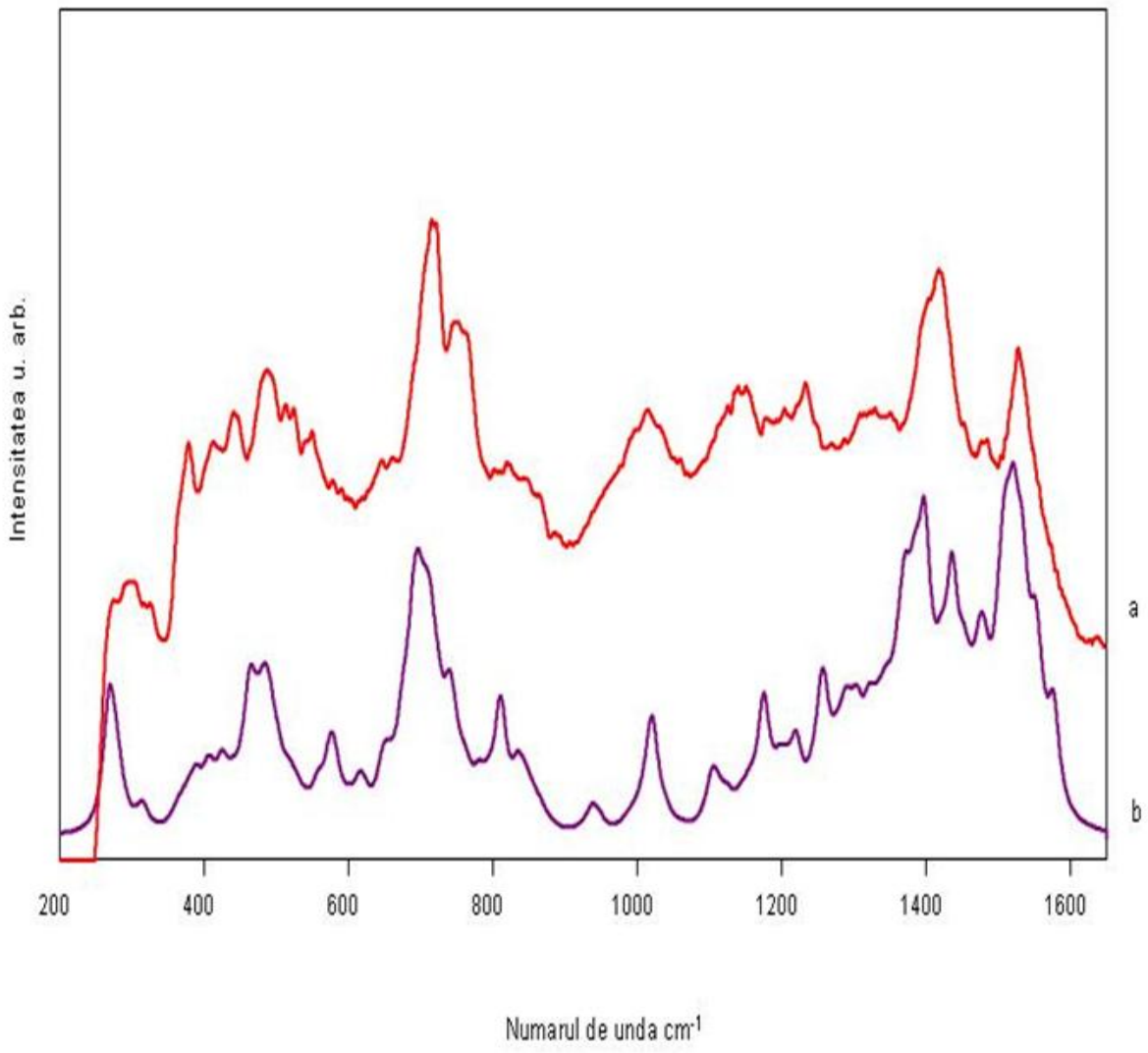

Figure 25. The SERS spectrum of the C_{50} film (red line) and the sum of simulated spectrum of the dimmers structure C_{50}-C_{50} (D_3) A and B (purple line)**.**

The combination of the spectra of the models considered when we started from the symmetrical monomer D_3 do not replay completely the spectrum obtained through experiments. All these changes show clearly an interaction between the molecules of C_{50} and the gold particles (or interaction with the SERS substrate), but one of the possible reasons for which the replay with the experiment is not possible is due to the fact that in the newly created material there are probably few traces of the C_{50} (D_3) isomer.

In the following spectrum is presented the sum of simulated spectra of the dimers structures of C_{50}-C_{50} (that were built starting from the monomers C_{50} with symmetry D_{5h} and D_3) with different positions of the gold atom and also with experimental spectrum of C_{50} SERS

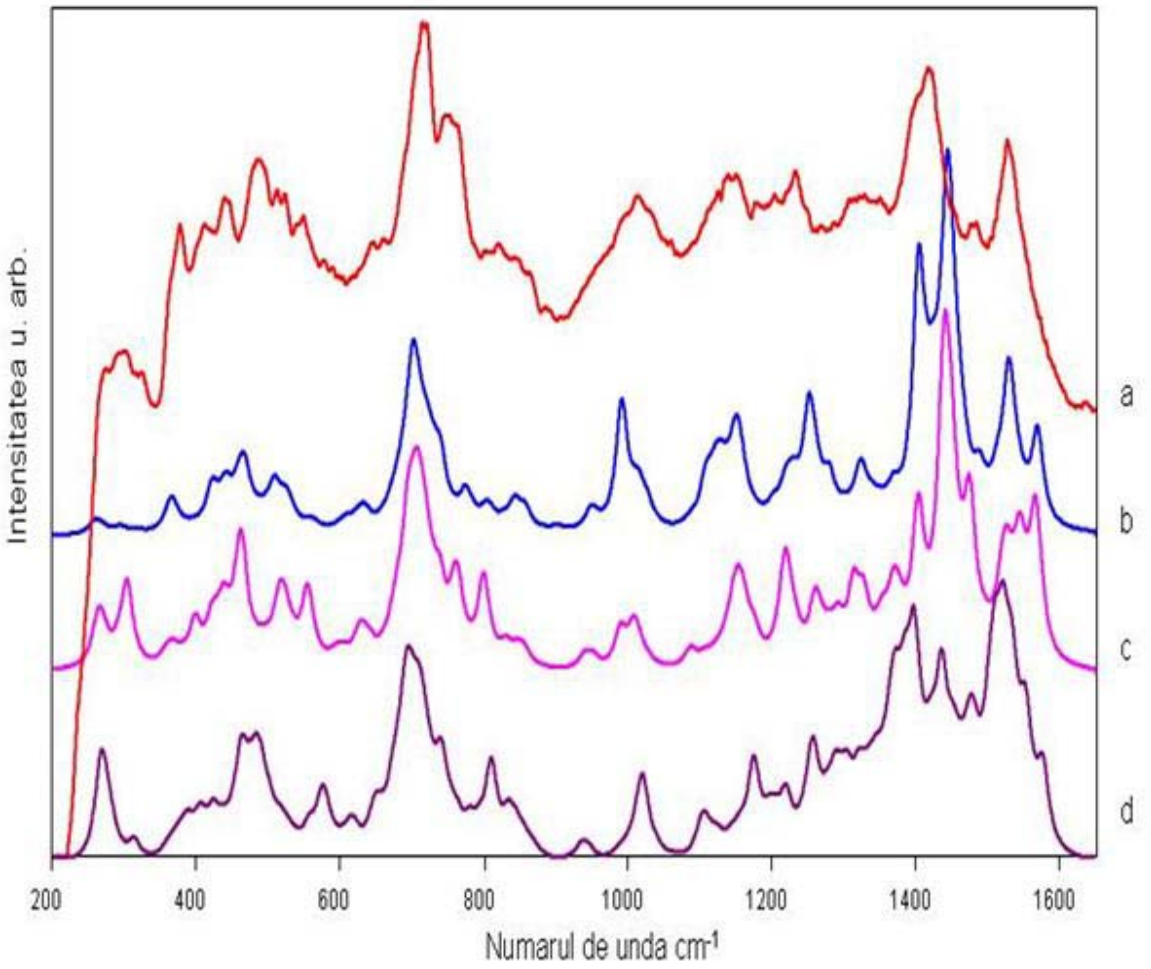

Figure 26. a) The spectrum SERS of C_{50} SERS (red line), b) the sum of simulated Raman spectrum of dimers structures C_{50}-C_{50} (D_{5h}) A and B (blue line), c) the sum of simulated Raman spectrum of dimers C_{50}-C_{50} (D_{5h}) C and D, d) the sum of simulated Raman spectrum of dimers C_{50}-C_{50} (D_3) A and B.

The significant modifications can be noticed in the positions and intensities of bands comparing the SERS spectrum of film C_{50} and the sum of Raman spectra of dimers structures (C_{50}-C_{50} (D_{5h}) A and B (blue line), C_{50}-C_{50} (D_{5h}) (C and D) and also C_{50}-C_{50} (D_3) (A and B). As we can notice from the spectra above the sum of spectra starting from monomer D_{5h}, positions A and B of the gold atom replay better the experimental spectrum of C_{50} SERS.

2.2.3.5 $C_{60}H_{21}F_9$

In this part we focus on obtaining new materials, starting from $C_{60}H_{21}F_9$ molecule, synthesized by Kabdulov and collaborators. In the group headed by Prof. Kappes (Karlsruhe University) they achieved to depose the precursor $C_{60}H_{21}F_9$ on a surface of HOPG. Raman spectra were made at room temperature using a thick film of $C_{60}H_{21}F_9$ deposed on a surface of HOPG.

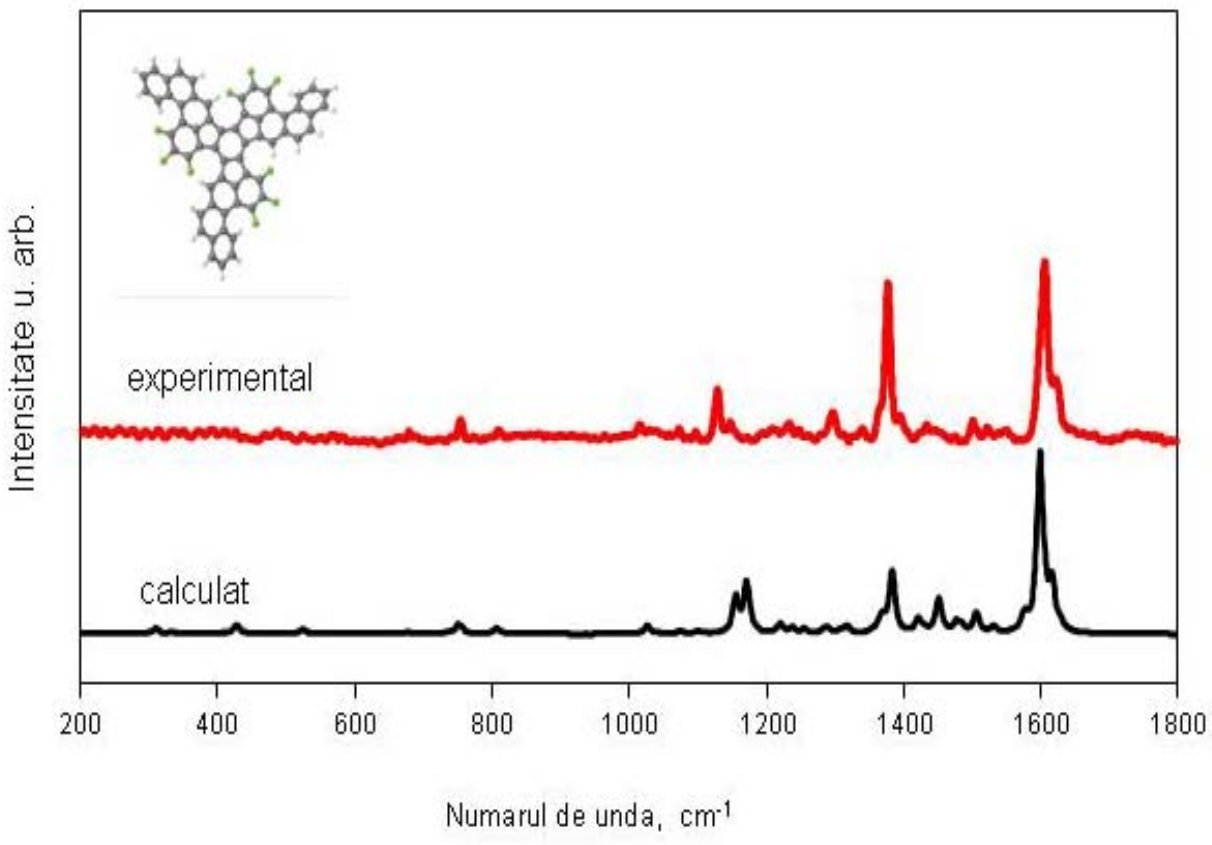

Figure 27. Comparison between Raman calculated spectrum (black line) and the experimental one of the film $C_{60}H_{21}F_9$ (red line).

Comparing the Raman spectrum of $C_{60}H_{21}F_9$ obtained through experiment to the absorption spectrum obtained after computation (DFT, TURBOMOLE 6.2, with functional BP86 and the basic set def-SV(P)), the connection between structure and spectrum can be noticed. Both spectra present the same vibrational modes. The calculations were done on an isolated molecule, without including the molecular interactions with the others. Despite this difference, the compliance between theory and experiment is almost perfect, fact that encourages us to continue this activity and to apply this strategy for other systems.

2.3 Conclusions

In this part I have developed a general methodology which helps to dissolve the molecular structure of fullerene clusters using the vibrational spectra that were obtained through experiments and also the calculations of density theory (DFT).

In order to explain the experimental spectra and to identify the non-IPR fullerene geometry of the fullerenic material there were calculations done using the density functional theory (DFT) both for monomers and for the dimers focusing especially on Raman and IR spectra. The starting geometry of fullerenes was obtained using the CaGe program. The computations were done using the Turbomole[10] software followed by the RI-DFT method with the Becke-Perdew (BP86) functional, using two basic sets: *def-SV(P)* and *def2-SV(P)* to calculate the structure and the vibrational spectra. The wavelength that was used to calculate the Raman spectrum was of 785 nm.

I supposed the vibronic properties of the oligomers that form the fullerene films could be described using the dimers C_n-C_n (it is too uneconomical to calculate the long oligomers). This strategy is reasonable to see the relation between theory and experiment.

Then the IR spectra calculated for neutral molecules, cations and anions were compared, so we can notice the difference between the spectra of the analysed species. With the simulated spectra could be identified the spectral lines of the species existing in the spectrum obtained through experiment. The analysis of the IR spectra that were obtained through experiment for different species of the fullerene C_{60} is possible by assigning absorption lines obtained after the calculation using the DFT method.

In order to reconstruct the Raman spectrum obtained through experiment for the film of C_{58} I created structural models starting from the isomers of the fullerene C_{58} that have the lowest energies. Starting from monomers C_{58} with symmetry: C_s, C_{3v} and C_2 I created dimers and I considered the cicloaddition process [2+2]. In order to connect the cages between them I considered more types of bonds. I obtained the Raman spectra of dimers C_{58}-C_{58}, with different bond possibilities. With the help of Raman spectra the vibration modes of the fullerenic material C_{58} could be differentiated, material that was obtained through experiment, comparing it to the Raman spectra of different dimers considered and also the difference between the dimers formed with different bond possibilities.

The Raman spectra of the oxidized film of C_{60} obtained through experiments have also been simulated. More DFT calculations have been done at theoretical level BP86 with the basic set def-SV(P) for molecular structures like: C_{60}, $C_{60}O$, $C_{60}O_5$, dimer C_{60}-C_{60}, complex C_{60}-O-C_{60},

complex C_{60}-O-C_{60}-O-C_{60}. Surprisingly, the oxidized spectrum of the film C_{60} is dominated by strong spectral features that are characteristic to clean spectrum C_{60} (thin films). All the Hg and Ag modes outlive the oxidation procedure. Comparing the simulated spectrum to the one that was obtained through experiment experimental of the complex C_{60} there occur some changes that are represented with the grey line. However, we found a unique characteristic of derivative oxygen which can be noticed in the spectrum below. In the area 1300-1600 cm^{-1} in the experimental spectrum $C_{60}O$ (red) a new band occur which can reproduce with the help of the simulated spectrum through the sum of all simulated Raman spectra for the considered models, illustrating an almost perfect reproduction with derivative shoulder for centred oxygen from 1458 cm^{-1}.

In order to help to characterize the experimental spectra of all fullerenes C_{60} and C_{50} from the fullerenic material deposited on the SERS substrate, I assessed the calculated vibrational frequencies with the experimental ones of the neutral species. In order to explain the SERS effect I calculated the vibrational frequencies:

a) For a better explanation of the SERS effect and to understand the interaction of molecule C_{60} with the SERS substrate (deposited on Klarite a Au-SERS substrate), I calculated the vibrational spectra of the molecule C_{60} with an atom of gold. The vibrational modes that occurred in the experimental spectrum of the film C_{60} deposited on a SERS substrate could be explained being helped by the simulated spectrum of $C_{60}Au$. In conclusion, the number of the vibrational modes is higher in the spectrum of film C_{60} deposited on a SERS substrate and this spectrum could get reproduced with the help of the simulated spectrum for fullerene C_{60} with gold atom. When the molecules of C_{60} are adsorbed on a gold surface the I_h symmetry of the molecule C_{60} is reduced. For this reason there is a fragmentation of Raman bands and there is a degeneration of the vibrational modes.
b) Comparing the theoretical spectra obtained for the six structural models of the dimer C_{50}-C_{50} with different positions of the gold atom (starting from the two isomers C_{50} with D_{5h} and D_3 symmetry) to the experimental spectrum of the film C_{50} deposited o6n a SERS substrate, the following conclusions can be drawn: from the structural models of dimer C_{50}-C_{50} (starting from the monomer C_{50} with D_{5h} symmetry) different positions of the gold atom on the surface of the cage A, B, C and D the combination of A and B spectra give some theoretical bands that can be also found in the experimental spectrum. The structural models of dimer C_{50}-C_{50} (starting from the monomer C_{50} with D_3 symmetry) do not reproduce completely the experimental spectrum of the film C_{50} deposited on a substrate SERS substrate.

c) There is a very good conformity between the experimental Raman spectrum and the simulated spectrum obtained through DFT theoretical calculations of the planar structure $C_{60}H_{21}F_9$. The two spectra present the same vibrational modes and the conformity between theory and experiment was almost perfect.

3. Topological description of crystalline networks

The operations on maps are presented here, maps that were used in the construction of the basic unit of the new crystalline networks and also the topological description of these networks using the Omega polynomial.

3.1 Operations on maps

Several operations on maps are known and used for various purposes. A map M can be defined as a combinatorial representation of a closed surface.

3.2 Omega polynomial

The molecular graph can be represented through a sequence of numbers, a matrix, a polynomial or a number derived from these (called topological index). For a given structure these representations should be singular.

The enumeration polynomial was introduced in the Mathematic Chemistry by Hosoya, and the general form of this polynomial is:

$$P(G,x) = \sum_k p(G,k) \bullet x^k$$

where *p(G,k)* is the occurrence frequency of selections / partitions of properties of *G* graph, having *k* dimension present as *k* exponent.

The enumeration polynomial Omega is useful in the topological description of benzenoid structures. The *qoc* strips can describe the helicity of tori and of tubes with polyhex cover. The coefficient of the factor that has the exponent c=1 from the Omega polynomial has a topological use; it represents a topological index named n_p and gives the number of pentagons that occur in the case of small fullerenes as a destability factor.

3.3 Omega polynomials in crystal lattice

Networks of crystalline type are presented in this subchapter, networks that are topologically characterised by using the Omega polynomial.

3.3.1 Units of networks S_2CL

The network unit, named S_2CL, was built through a transformation with the sequence Tr(Du(Med(Le(Oct))) and is a triple periodic network. This operation sequence introduces triples of pentagons in a polygonal surface, which breaks the isolated pentagon rule (IPR-Isolated Pentagon Rule), a stability condition in the case of the classical fullerenes.

The lattice under study named S_2CL, was designed by the sequence Tr(Du(Med(Le(Oct))); and is a triple periodic network. In the above sequence, Tr means the truncation of some selected vertices. This sequence violate the IPR (Isolated Pentagon Rule) condition in fullerene stability.

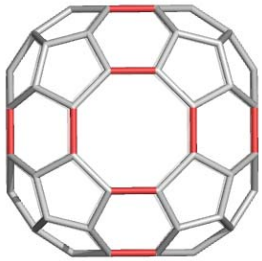

111

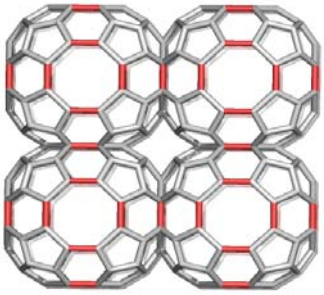

222

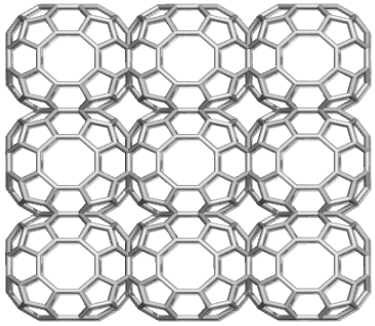

333

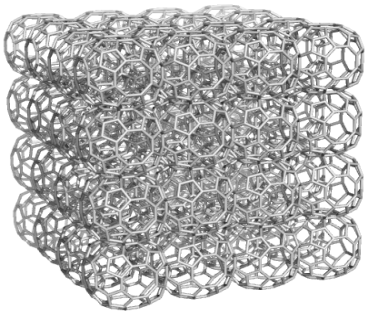

444

Figure 28. Lattice S_2CL; units designed by *Tr*(*Du*(*Med*(*Le*(Oct)))); the red bonds mark the octagonal faces to be identified in constructions of the networks.

In figure 28 can be noticed the unit of the lattice (111), and structural fields (kkk), ex. (222), (333), and (444), k is the number of repetitive units on each space dimension. The lattice S_2CL was obtained identifying the units on octagonal sides. In this way there occurs the canals regulation like those from zeolites. The topological description of the lattice S_2CL was done using the Omega polynomial, and in table 1 are the analytical formulae to calculate the Omega polynomial in an infinite lattice S_2CL and also examples of numerical calculations.

We used here the topological description by Omega polynomial because this polynomial was created to describe the covering in polyhedral nanostructures and because it is the constitutive part of nanostructures, particularly for large structures, with a minimal computational cost.

Formulas for Omega polynomial in S_2CL network and examples are given in Table 1.

Table 1. Omega polynomial in S_2CL;R_{max}=8.

Formulas
$\Omega(S2CL,x)=24a^3\cdot x^1+6a(a^2+9a-4)\cdot x^2+12a(a-1)^2\cdot x^4+3a\cdot x^{a(8+4(a-1))}$
$\Omega'(S2CL,1)=24a^2(4a+1)$
$\Omega''(S2CL,1)=48a(a^4+2a^3+4a^2-4a+2)$
$CI(S2CL)=24a(384a^5+190a^4+20a^3-12a^2+7a-4)$

Examples		
Net	Omega	CI
111	$24x+36x^2+3x^8$	14040
222	$192x+216x^2+24x^4+6x^{24}$	741600
333	$648x+576x^2+144x^4+9x^{48}$	7858872
777	$8232x+4536x^2+3024x^4+21x^{224}$	1161954360
888	$12288+6336x^2+4704x^4+24x^{288}$	2567169792

Data were calculated by the original software Nano-Studio, developed at TOPO Group Cluj, Romania. The design of the hypothetical crystalline structure S_2CL was performed using the operations on maps. The aim of this network is to simulate the channels that occur in some zeolites. The topology of the proposed network was described using the Omega polynomial.

3.3.2. Units of network Tr(P_4(M)

The lattice was constructed by using a basic unit, designed with a net operation sequence on maps, Tr(P_4(M)), where M=Oct (Octahedron) .

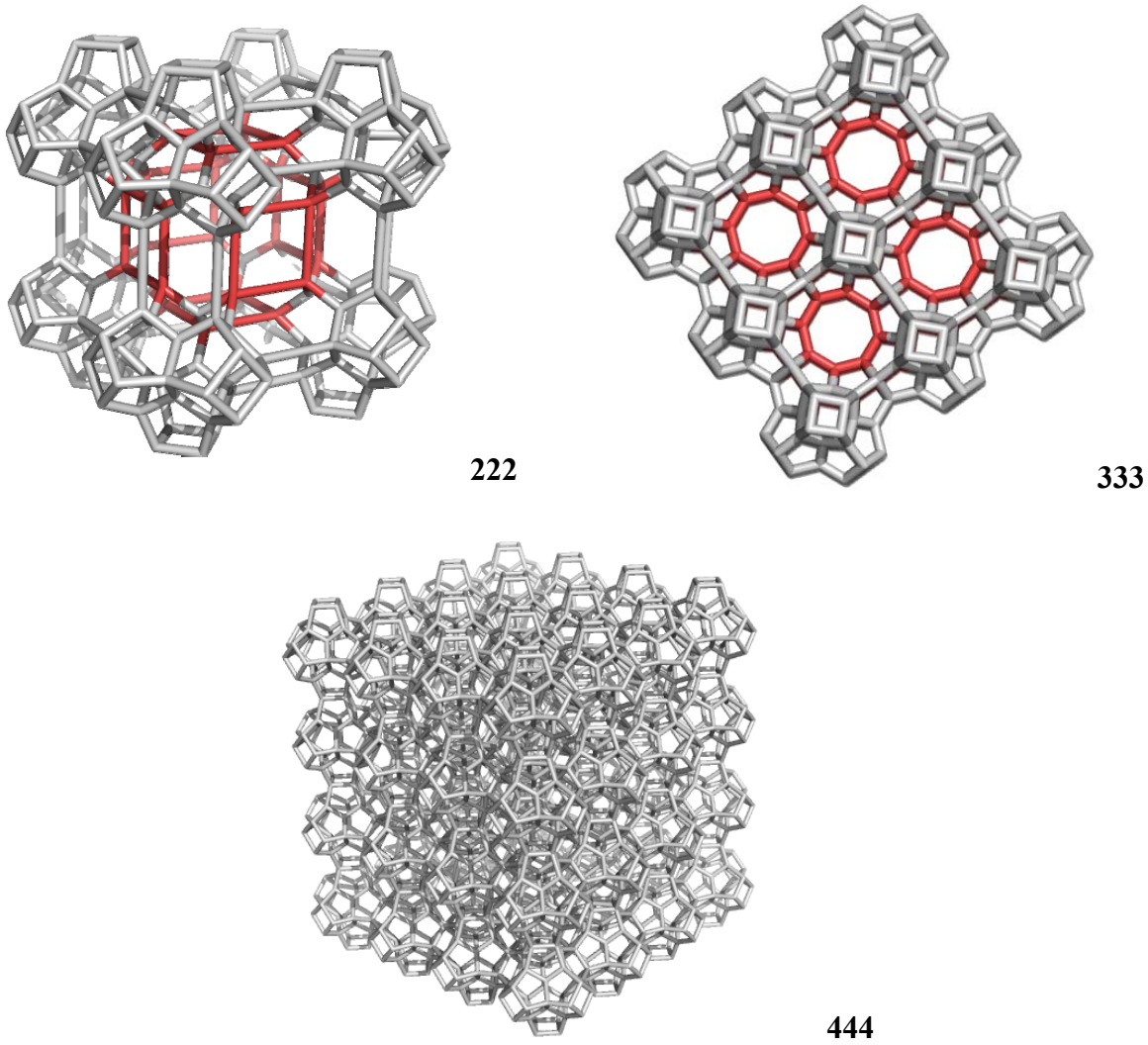

Figure 29. Network Tr(P_4(M)) (222, 333, 444), M=Octahedron, in two different views.

The net (Figure 29) was built up by identifying the identical (quadrilateral) faces of unit structure. The crystal-like structure shows oriented hollows, as those encountered in zeolites, natural alumino-silicates widely used in synthetic chemistry as catalysts

The units involved in these constructions, namely Tr(P_4(M)), M=Oct, as a hydrogenated structure, shows moderate stability as given by their heat of formation HF, total energy TE and HOMO-LUMO, calculated at the PM3 level of theory (Table 3).

For example, the total energy per heavy atoms of the structures in Table 2 and Figure 30 are between the values of adamantane (-3305.19 kcal/mol), which is the most related small structure and C_{60} (-2722.45 kcal/mol), the standard molecule in nanostructures. The same is true about the HOMO-LUMO gap. Calculations by using a density functional-based tight binding method combined with the self-consistent charge technique (SCC-DFTB) on hydrogenated units of diamond and diamond-like[18] networks have shown the same ordering of stability as given by PM3 approach; thus our results reported here can be considered as pertinent ones.

Table 2**.** Quantum Chemistry PM3 data for some units designed by Tr(P_4(M)). Heat of Formation HF, Total energy TE and HOMO-LUMO Gap HLGAP

M	N-heavy atoms	HF (kcal/mol)	HF/N heavy	TE (kcal/mol)	TE/Ni	HLGAP (eV)	Sym.
Ico	**110**	**1216.81**	**11.06**	**-328026**	**-2982.05**	**11.79**	**I_h**
Oct	**44**	**448.67**	**10.19**	**-131248**	**-2982.92**	**12.17**	**O_h**
T	**22**	**308.48**	**14.022**	**-65540**	**-2979.09**	**11.99**	**T_d**

The Omega polynomial (calculated at R_{max}[8]) for the investigated networks Tr(P_4(M)) is as follows:

$$\Omega(G,x) = 24a(a+1)x + 12(a(a+1)+(a-2))x^2 + 24(a(a-2)+1)x^3 + 4(a-1)^3 x^6 + 3(a-1)x^{(2a)^2}$$

$$\Omega'(G,1) = |E(G)| = 36a^2(a+1)$$

$$CI(G) = 1296a^6 + 2544a^5 + 1344a^4 - 144a^3 + 144a^2 - 120a + 24$$

The above formulas can be verified with the examples listed in Table 3.

Table 3. Examples of Omega polynomial and CI calculation.

A	Omega polynomial	CI
1	$48x+12x^2$	5088
2	$144x+72x^2+24x^3+4x^6+3x^{16}$	185064
3	$288x+156x^2+96x^3+32x^6+6x^{36}$	1668912
4	$480x+264x^2+216x^3+108x^6+9x^{64}$	8250168
5	$720x+396x^2+384x^3+256x^6+12x^{100}$	29025024
6	$1008x+552x^2+600x^3+500x^6+15x^{144}$	81963528

Calculations were performed by our Nano Studio software program. In figure 30 are represented platonic structures transformed by $Tr(P_4(M)$ sequence of map operations: M=Tetrahedron T (left); M=Octahedron Oct (central) and M=Icosahedron Ico (right). The red colour is only to show the related substructures.

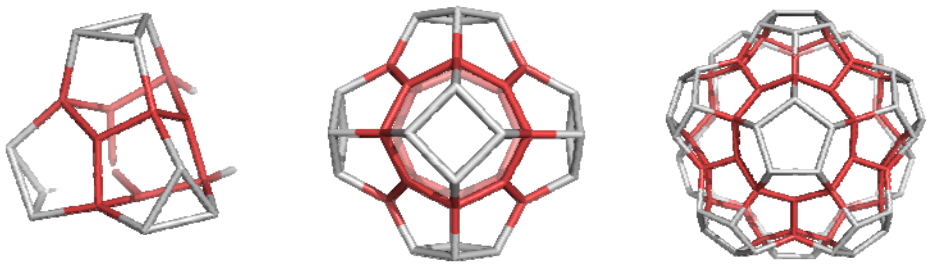

Figure 30. Platonic structures transformed by $Tr(P_4(M))$.

A hypothetical crystal networks was built up by using a repeated unit designed by $Tr(P_4(M))$ sequence of map operations. It was shown that the octahedral monomer (i.e., the repeated unit of these networks) is the most stable (as hydrogenated species) among the similar structures derived from the Platonic solids, and all these have a moderate stability, between adamantane and C_{60} fullerene, as calculated at the PM3 level of theory. The topology of the networks was described in terms of Omega polynomial, function of the net parameters

.

3.3.3 Other crystal networks

The nets herein discussed were built up by combination of map operations.

3.3.3.1 Net A

The unit of this net is an isomer of cuboctahedron (which is the medial of Cube and Octahedron). The net is constructed by identifying some squares (Figure 31) so that net appears as "translated" on Z-axis, each time one row. The computed data for the Omega polynomial of this net were rationalized as in the formulas presented below:

$$\Omega(G,x) = 4a(2a-1)x^{1} + (2a^{3} + 7a^{2} + 3a - 4)x^{2}$$
$$+ ax^{2a(a+2)} + ax^{3a(a+1)} + (a-1)x^{4(a-1)(3a+2)}$$

$$|E(G)| = \Omega'(G,1) = 21a^{3} + 13a^{2} - 2a$$

$$CI(G) = 441a^{6} + 389a^{5} + 291a^{4} - 5a^{3} - 272a^{2} - 8a + 80$$

Examples to verify the formulas are shown in Table 4.

Table 4. Omega polynomial and Index CI for A net, examples

A	Omega	CI
1	$4x^{1}+8x^{2}+2x^{6}$	916
2	$24x^{1}+46x^{2}+2x^{16}+2x^{16}+2x^{18}+1x^{32}$	44264
3	$60x^{1}+122x^{2}+3x^{30}+3x^{36}+2x^{88}$	437060
4	$112x^{1}+248x^{2}+4x^{48}+4x^{60}+3x^{168}$	2274544
5	$180x^{1}+436x^{2}+5x^{70}+5x^{90}+4x^{272}$	8280740
6	$264x^{1}+698x^{2}+6x^{96}+6x^{126}+5x^{400}$	23966456
7	$364x^{1}+1046x^{2}+7x^{126}+7x^{168}+6x^{552}$	59104804
8	$480x^{1}+1492x^{2}+8x^{160}+8x^{216}+7x^{728}$	129524240

In figure 31 is the net unit (111a and 111b) and the branch made up of 3 units (333a and 333b), on each dimension.

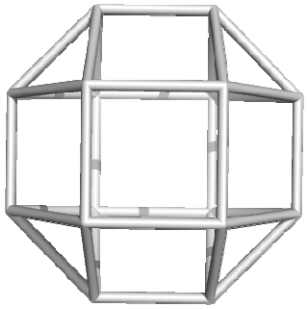

111a

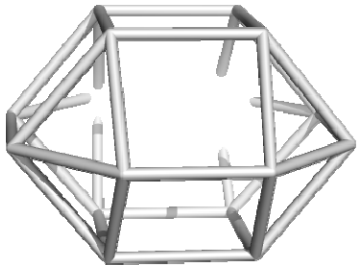

111b

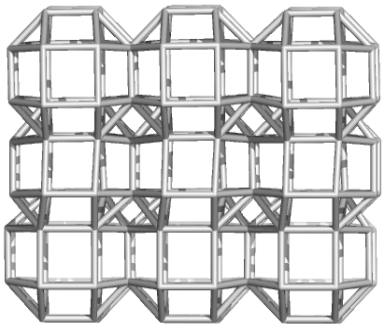

333a

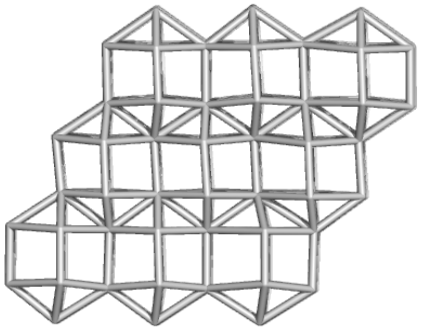

333b

Figure 31. Net A, unit 111 (top) and 333 (bottom).

3.3.3.2 Units B

The unit of this net is as for the case A but the edges sharing triangles were deleted. Moreover, the net is constructed being translated on only two directions (Figure 32). Note, these networks are only double periodical, as can be seen in the bottom rows of figures. The computed data for the Omega polynomial of this net were rationalized as in the formulas presented below and Table 5.

$$\Omega(G,x) = 4\sum_{i=1}^{a-1} x^{(10+4(a-2))i} + 2x^{2a(2a+1)} + 1x^{16a^3}$$

$$|E(G)| = \Omega'(G,1) = 4a^2(6a+1)$$

$$|V(G)| = 8a^2(a+1)$$

$$\Omega''(G,1) = 245a^6 + \frac{64}{3}a^5 + \frac{64}{3}a^5 - 8a^3 + \frac{20}{3}a^2 - \frac{8}{3}a$$

$$CI\ (G) = 320a^6 + \frac{512}{3}a^5 - \frac{16}{3}a^4 - 16a^3 + \frac{32}{3}a^2 - \frac{8}{3}a$$

$$= \frac{8}{3}a\left(120a^5 + 64a^4 - 2a^3 - 8a^2 - 4a - 1\right)$$

Table 5. Omega polynomial and Cluj-Ilmeneau (CI) index of the Net B: Examples

A	Omega Polynomial	CI
1	$2x^6+2x^8$	584
2	$4x^{10}+2x^{20}+1x^{128}$	25680
3	$4x^{14}+4x^{28}+2x^{42}+1x^{432}$	273784
4	$4x^{18}+4x^{36}+4x^{54}+2x^{72}+1x^{1024}$	1482912
5	$4x^{22}+4x^{44}+4x^{66}+4x^{88}+2x^{110}+1x^{2000}$	5527720
6	$4x^{26}+4x^{52}+4x^{78}+4x^{104}+4x^{130}+2x^{156}+1x^{3456}$	16246256
7	$4x^{30}+4x^{60}+4x^{90}+4x^{120}+4x^{150}+4x^{180}+2x^{210}+1x^{5488}$	40497240
8	$4x^{34}+4x^{68}+4x^{102}+4x^{136}+4x^{170}+4x^{204}+4x^{238}+2x^{272}+1x^{8192}$	89447744

In figure 32 is shown the unit of B network (111a and 111b) and a branch with 2 units each, (222a and 222b), on each dimension.

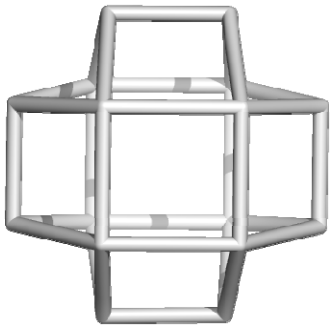

111a

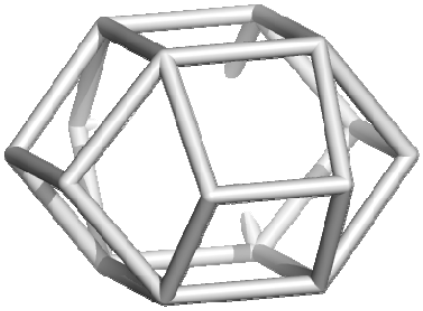

111b

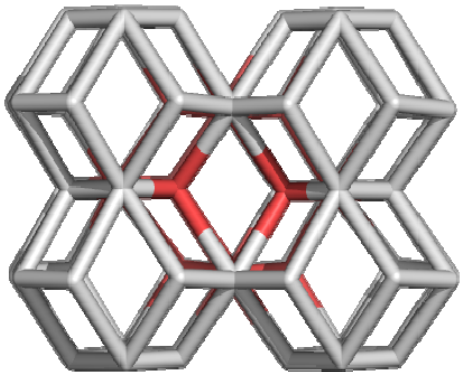

222a

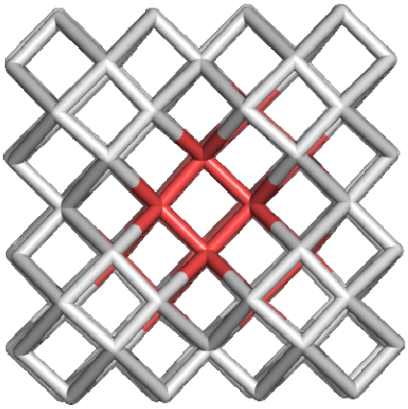

222b

Figure 32. Net B unit 111 (top) and 222 (bottom).

Omega polynomial can be used in topological description of polyhedral crystal networks.

3.4 Conclusions

Being helped by the map operations and using the Nano Studio software to connect the basic units, it was possible to obtain four new crystalline networks that were then topologically characterised using the Omega polynomial.

For example:

■ the network unit named S_2CL was built through a sequence transformation Tr(Du(Med(Le(Oct))) and represents a triple periodic network;

■ for the network $Tr(P_4(M))$ we started from an octahedron that is the basic unit, followed by a number of map operations and then the network was built identifying the quadrilateral sides;

■ The difference between A and B networks consists in the face that one is constructed by identifying some squares (network A), while B network is made up by erasing the triangle edges from A network. B network is translatable only on 2 directions, so it is a double-periodic network. For both networks we started from a cuboctahedron isomer which is the medial of Cube and Octahedron.

The new constructed structures, of crystal type, have oriented gaps, like those from the natural zeolites, largely used in chemical synthesis. While constructing the crystalline networks, the following programmes were used: CVNET, to modify the fullerene cover, Nano Studio to connect the units of the networks and to compute the Omega polynomial.

4. Conclusions

In the last years there has been a great interest in producing fullerenic materials, with important technical applications.

This PhD thesis especially the original contributions, focuses on two directions:

1. DFT calculations for fullerenes (Chapter 2).
2. Topological description of crystalline networks (Chapter. 3).

In the part referring to DFT calculations for fullerenes I developed a general methodology that allows to elucidate the molecular structures of fullerene clusters using the vibrational spectra obtained through experiments and also calculations of density functional theory (DFT). This research is aimed to identify the Raman and IR bands and also to identify the IPR and non-IPR fullerene geometry of the fullerenic material. The calculations were performed using the density functional theory (DFT), both for monomers and dimers, focusing more on the Raman and IR spectra. The starting fullerene geometry was obtained using the CaGe software. The computation was performed using the Turbomole software, followed by RI-DFT method with Becke-Perdew (BP86) functional, using two basic sets: *def-SV(P)* and *def2-SV(P)* to calculate the structure and the vibrational spectra. The wavelength that was used in the calculation of Raman spectrum was of 785 nm.

Helped by simulated spectra we could identify the spectral lines of the species that exist in the experimental spectrum. The analysis of the experimental IR spectra of different species of fullerene C_{60} is possible by assigning the absorption lines obtained after calculation through DFT method.

In order to simulate the experimental Raman spectrum of the film C_{58} I created structural models starting from isomers of fullerene C_{58} which have the lowest energy. Starting from monomers C_{58} with symmetry: C_s, C_{3v} and C_2, I created dimers and the cicloaddition process was considered [2+2]. In order to connect the cages among them I considered more types of bonds. The Raman spectra of dimers C_{58}-C_{58} were obtained, with different bonds. Helped by Raman spectra I could differentiate the vibrational modes of the experimental fullerenic material C_{58} compared to the Raman spectra of different dimers considered, and also the differentiation among dimers with different bonds.

The Raman spectra of oxidized film C_{60} obtained through experiment were also simulated. Many theoretical DFT computations were performed with BP86 with the basic set def-SV(P), for many molecular structures like: C_{60}, $C_{60}O$, $C_{60}O_5$, dimer C_{60}-C_{60}, complex C_{60}-O-C_{60}, complex C_{60}-O-C_{60}-O-C_{60}. Surprisingly, the oxidized spectrum of film C_{60} is dominated by strong spectral features that are characteristic to spectrum C_{60} (thin films) clean. All the Hg and Ag modes outlive the oxidation procedure. Comparing the simulated spectrum and the experimental one of the complex of C_{60} there occur some modifications. However, I found a unique characteristic of derived oxygen which can be noticed in the spectrum below. In the 1300-1600 cm^{-1} area in the experimental spectrum $C_{60}O$ (red) there occur a new band which can reproduce, helped by the simulated spectrum namely through the sum of all Raman spectra simulated for the models considered. This show an almost perfect reproduction with derived shoulder for oxygen centred from 1458 cm^{-1}.

In order to help to characterise the experimental spectra of fullerenes C_{60} and C_{50} from the fullerenic material deposited on SERS substrate. I assessed the calculated vibrational frequencies with the experimental ones of the neutral species. In order to explain the SERS effect the vibrational frequencies were calculated:

a) For a better interpretation of the SERS effect, namely to understand the interaction of molecule C_{60} with the SERS substrate (deposited on Klarite a substrate Au-SERS), I calculated the vibrational spectra of molecule C_{60} with a gold atom. Helped by the simulated spectrum C_{60}Au I could explain the vibrational modes that occurred in the experimental spectrum of film C_{60} deposited on a SERS substrate. In conclusion, the number of vibrational modes is increased in the spectrum of film C_{60} deposited on a SERS substrate and this spectrum could reproduce helped by the simulated spectrum for the fullerene C_{60} with gold atom. When the molecules of C_{60} are adsorbed on a gold surface, the I_h symmetry of molecule C_{60} is reduced, and for this reason there occur a fragmentation of Raman bands and also a degeneration of vibrational modes.

b) Comparing the theoretical spectra obtained for the six structural models of dimer C_{50}-C_{50} with different positions of the gold atom (starting from the two isomers C_{50} with symmetry D_{5h} and D_3) to the experimental spectrum of film C_{50} deposited on a SERS substrate we can conclude: from the structural models of dimer C_{50}-C_{50} (starting from monomer C_{50} with symmetry D_{5h}) different positions of the gold atom on the cage surface A, B, C and D the combination of spectra A and B give some theoretical bands that can be found in the experimental spectrum, and the structural models of the dimer C_{50}-C_{50} (starting from monomer C_{50} with symmetry D_3 do not totally reproduce the experimental spectrum of film C_{50} deposited on a SERS substrate.

There is a very good conformity between the Raman experimental spectrum and the simulated spectrum obtained through theoretical DFT computation of the planar structure $C_{60}H_{21}F_9$. The two spectra present the same vibrational modes so the conformity between theory and practice is almost perfect. Despite some small differences, there could be noticed a complete conformity between theory and experiment, fact that encourages us to continue our activity and to apply this strategy for other systems, too.

In the second part of description of crystalline networks, there were modelled four new crystalline networks which were then topologically characterised using the Omega polynomial.

- the net unit called S_2CL was constructed through a transformation with the sequence Tr(Du(Med(Le(Oct))) and represents a triple periodic network;
- the net $Tr(P_4(M))$ started from octahedron which is the basic unit, followed by a succession of operations on maps, then the network was constructed by identification of quadrilateral sides;
- the difference between **A** and **B** networks is that one is constructed by identifying some squares (network A), while network B is made up by deleting the edges of the triangles of network A. Network B is translatable only on two directions and is a double periodic network. For both networks we started from a cuboctahedron isomer which is the medial of Cube and Octahedron. I also determined the analytical formulae of these crystalline networks.

The results obtained for the topological description of the crystalline networks were published in Studia Universitatis Babes-Bolyai Chemia.

Selected bibliography

1. H.W. Kroto, *Nature,* 314, 162, **1985**.
2. S. Iijima, *Nature*, 354, 56, **1991**.
3. K. S. Novoselov, A. K. Geim, *Science*, 306, 666, **2004**.
4. D. Löffler, S. S. Jester, P. Weis, A. Böttcher, M. M. Kappes, *J. Chem. Phys*, 124, 054705, **2006**.
5. D. Löffler, N. Bajales, M. Cudaj, P. Weis, S. Lebedkin, A. Bihlmeier, D. P. Tew, W. Klopper, A. Böttcher, M. M. Kappes*, J. Chem. Phys.*, 130, 164705, **2009**.
6. A. Böttcher, P. Weis, S. S. Jester, D. Löffler, A. Bihlmeier, W. Klopper, M. M. Kappes, *Phys. Chem. Chem. Phys.*, 7, 2816, **2005**.
7. D. Löffler, S. Ulas, S. S. Jester, P. Weis, A. Böttcher, M. M. Kappes, *Phys. Chem. Chem. Phys.*, 12, 10671, **2010.**
8. G. Brikmann, O. Delgado Friedrichs, A. Dress, T. Harmuth. *Match*., 36, 233, **1997.**
9. G. Brikmann, O. Delgado Friedrichs, S. Lisken, A. Peeters, N. Van Cleemput, *Match*, 63, 533, **2010.**
10. J. J. P Stewart*, J. Mol. Model.,* 10 (2), 155, **2004**.
11. J. J. P Stewart*, J. Mol. Model.,* 13 (12), 1173, **2007**.
12. Turbomole, versiunea 6.2 (2010), Turbomole Gmb, Karlsruhe, http://www.turbomole.com
13. O. Vahtras, J. Almlöf, M. W. Feyereisen, *Chem. Phys. Lett*., 213, 514, **1993**.
14. J. Fulara, M. Jakobi, J. P. Maier*, Chem. Phys. Lett*., 211, 227, **1993.**
15. B. Kern, ..., M. M. Kappes, Karlsruhe Institut of Technologie, în pregătire.
16. A. Bihlmeier, W. Klopper, *Phys. Chem. Chem. Phys.*, 11, 1050, **2009**.
17. M. J. Rice, H. Y. Chai, *Phys. Rev. B*, 45, 10173, **1991**.
18. S. Ulas, ..., M. M. Kappes, Karlsruhe Institut of Technologie, în pregătire.
19. S. Ulas, M. Cudaj, D. Löffler, N. Bajales Luna, M. L. Pop, D. Strelnikov, A. Böttcher, M. Kappes, Atomic oxidation of C_{60} films: Thermal stability of the oxyfullerides, în pregătire.
20. Y. Fang, Q.-J. Huang, P. Wang, Xiao-Yuan Li, Nai-Teng Yu, *Chem. Phys. Lett*., 381, 255, **2003.**
21. L. Zhixum, F. Yan, *Vibrational Spectroscopy*, 39, 151-156, **2005.**

22. P. W. Folwer, D. E. Manolopolos, *An Atlas of Fullerenes, The Clarendon Press*, Oxford, **1995**.
23. X. Zaho, *J. Phys. Chem. B*., 109, 5267, **2005**.
24. S. Y. Xie, F. Gao, X. Lu, R. B. Hung, C.- R. Wang, X. Zhang, M. L. Liu, S. L. Deng, L. S. Zheng, *Science*, 304, 699, **2004**.
25. M. A. Kabdulov, K. Y. Amsharov, M. Jansen, *Tetrahedron*, 66, 8587, **2010**.
26. P. W. Fowler, T. Pisanki, *J. Chem. Soc. Faraday Trans*., 90, 2865, **1994**.
27. T. Pisanski, M. Randic, *Bridges between geometry and graph theory, in Geometry at Work, M. A. A. Notes,* 53, 174, **2000**.
28. H. Hosoya*, Bull. Chem. Soc. Japan*, 44, 2332, **1971**.
29. H. Hosoya, *Discrete Appl. Math*., 19, 239, **1998**.
30. H. W. Kroto, *Nature*, 329, 529, **1987**.
31. X. Han, S. J. Zhou, Y. Z. Tan, X. Wu, F. Gao, Z. J. Lio, R. B. Huang, Y. Q. Feng, X. Lu, S. Y. Xie, L. S. Zheng, *Angew. Chem. Int. Ed*., 47, 5340, **2008**.
32. L. Carlucci, G. Ciani, D. Proserpio, *Coord. Chem. Rev*., 246, 247, **2007**.
33. M. Saheli, R. O. Pop, M. L. Pop, M. V. Diudea, *Studia Universitatis Babes-Bolyai Chemia*, 4, 241, **2010**.
34. M. V. Diudea, A. Bende, D. Janeić, *Fullerenes, Nanotubes, Carbon Nanostruct*., 18 (3), 236, **2010.**
35. V. A. Blatov, L. Carlucci, G. Giani, D. Proserpio, *Cryst. Eng. Comm*., 6, 377, **2004**.
36. Cs. L. Nagy, M. V. Diudea, *Nano Studio software*, Babeş-Bolyai Univ., **2009**.
37. M. Saheli, M. Ghorbani. M. L. Pop, M. V. Diudea, *Studia Universitatis Babes-Bolyai Chemia*, 4, 241, **2010**.
38. M. V. Diudea, S. Cigher, A. E. Vizitiu, M. S. Folerescu, P. John, *J. Math. Comput. Chem*., 60, 965, **2008**.

List of publications

1. M. L. Pop, M. V. Diudea, Topology of a new lattice containing pentagon triples, *Studia Universitatis Babes-Bolyai Chemia*, 199-206, **2010.**
2. M. Saheli, R. O. Pop, M. L. Pop, M. V. Diudea, Omega polynomial in Oct-P_4TRS Network, *Studia Universitatis Babes-Bolyai Chemia*, 215-218, **2010**.
3. M. Saheli, M. Gorbani, M. L. Pop, M. V. Diudea, Omega polynomial in crystal-like networks, *Studia Universitatis Babes-Bolyai Chemia*, 241-246, **2010**.
4. M. L. Pop, M. V. Diudea, A. Ilic, Correlating study of new molecular graph descriptors, *Studia Universitatis Babes-Bolyai Chemia*, 19-25, **2010**.
5. M. V. Diudea, K. Nagy, M. L. Pop, F. Gholami-Nezhaad, A.R. Ashrafi, Omega and PI_y polynomial in Dyck graph-like Z(8) unit networks, *Int. J. Nanosci. Nanotechnol*., 97-103, **2010**.

Comunications:

1. ICAM "Mathematical Chemistry in Nano-Era" Minisymposium,
   1-4 September, Cluj-Napoca, **2010**.
   Topology of pentagon triples containing lattice-poster
2. The First Iranian Conference on Chemical Graph Theory,
   6-7 October, Theran, Iran, **2010.**
   Omega polynomial in crystal-like networks-poster
3. Workshop Contract Posdru 6/1.5/S/3,
   30 September, Cluj-Napoca, **2010**.
   Descrierea topologică a laturilor pentagoane triple-prezentare

Acknowledgements

The present thesis is a result of studies performed in TOPO group Cluj, headed by Prof. Dr, Mircea V. Diudea, from the Organic Chemistry Department of Faculty of Chemistry and Chemical Engineering of "Babes-Bolyai" University Cluj Napoca, and also of studies of the German group headed by Prof. Manfred Kappes Ph.D, from Karlsruhe Institut of Technology (KIT), Germany.

On the occasion of finishing this work which represents the essence of my research activity, I would like to thank all those who guided me and shared their professional knowledge and their experimental abilities, offered me moral support, and encouraged me in difficult moments.

Furthermore, I would like to thank Prof. Dr. Mircea V. Diudea, for accepting me as Ph.D student and for offering me the chance to finish the work I started. I would also like to thank him for the understanding and trust he gave me during the time when I worked in the team he headed.

I want to express my special thanks to Prof. Dr. Manfred M. Kappes from Karlsruhe Institut of Technology (KIT), Germany, for his amiability to accept me to do the research in his group.

I have many thanks and consideration to Dr. Artur Böttcher, Dr. Dmitry Strelnikov, Seyithan Ulas and Bastian Kern for offering a warm environment and for scientific support.

To my colleagues Dr. Nagy Csaba, Dr. Nagy Katalin, Lect. Dr. Gabriel Katona, Tasnadi Erika, Fustos Melinda, Bucila Virginia, Pop Cristina, my thanks and consideration for the moral support offered during my Ph.D time.

I would like to thank for the financial support provided by the Programme co financed through the Human Resources Sectorial Programme 2007-2013, POSDRU Contract 6/1.5/S/3-Doctoral studies: Through Science and Society.

For the warmth and support regarding the time needed for this work and the help offered during the years, I thank my family.